AALBORG UNIVERSITY
STUDENT REPORT

Addressing recombinant AAV9 as a novel therapeutic strategy for gene correction of Niemann Pick's type C2 disease in the CNS

Master thesis by
Ida Køgs Andersen, Lissa Vestergaard Hauerslev and Lonnie Møller Johansen

School of Medicine and Health, Aalborg University 2019

AALBORG UNIVERSITY

STUDENT REPORT

Title of the thesis: Addressing recombinant AAV9 as a novel therapeutic strategy for gene correction of Niemann Pick's type C2 disease in the CNS

Field of study: Medicine with Industrial Specialization, Biomedicine

Group number: 9026

Supervisors: Assistant professor Annette Burkhart Larsen, Associate professor Louiza Bohn Thomsen

Co-supervisor: PhD student Eva Hede Olsen

Standard pages: 47

Appendices: 8

Project members signatures:

Ida Køgs Andersen

Lissa Vestergaard Hauerslev

Lonnie Møller Johansen

Resumé

Baggrund: Niemann Picks type C2 (NPC2) er en dødelig sygdom forårsaget af mutationer i NPC2 genet. Sygdommen påvirker centralnervesystemet, og eftersom adeno-associeret virus serotype 9 (AAV9) er neurotrofisk, kan den potentielt anvendes som en ny behandling af sygdommen ved at mediere genterapi, der introducerer et funktionelt NPC2-gen.

Formål: At evaluere AAV9-medieret genterapi mod Niemann Picks type C2 i centralnervesystemet.

Metoder: Rekombinant AAV9-NPC2-2A-GFP blev testet på en in-vitro blod-hjerne barriere (BHB) model bestående af primære hjerneendotelceller fra svin (SHEC) og primære rotteastrocytter. Transduktion af BHB-modellen blev evalueret 10 dage efter tilsætning af AAV9-NPC2-2A-GFP ved detektion af GFP-transgenet med immuncytokemi og RT-qPCR. Den potentielle terapeutiske effekt af AAV9-NPC2-2A-GFP blev undersøgt med en ELISA, der målte secerneret NPC2-protein. De mulige skadelige effekter af virus-tilsætningen blev evalueret med målinger af trans-endotel elektrisk modstand (TEEM) og immunfarvninger af Zona Occludens-1 (ZO-1) og GFAP.

Resultater: GFP kunne hverken detekteres i SHEC eller astrocytter, og mængden af secerneret NPC2 protein lå under detektionsgrænsen. TEEM-værdierne var signifikant lavere ved de AAV9-behandlede barrierer (n=9) sammenlignet med ubehandlede (n=9) fra dagen efter tilsætning af virus til og med 5.-dagen ($p<0,05$). GFAP-farvningen indikerede at astrocytterne var mere reaktive ved tilsætning af AAV9-NPC2-2A-GFP, men der var ingen forskelle at observere mellem behandlingerne i ZO-1-farvningen.

Konklusion: AAV9-NPC2-2A-GFP kunne ikke transducere BHB-modellen, og NPC2-secernering kunne ikke påvises. AAV9-NPC2-2A-GFP forringede tætheden af BHB-modellen.

Abstract

Background: Niemann Pick's type C2 (NPC2) is a fatal disease with neurological involvement caused by mutations in the NPC2 gene. Adeno associated virus serotype 9 (AAV9) is known to be neurotropic and may be used as a novel therapeutic strategy for this disease by gene correction of NPC2.

Objective: To evaluate AAV9-based gene therapy for NPC2 disease in the central nervous system.

Methods: Recombinant AAV9-NPC2-2A-GFP was tested on an in vitro non-contact blood brain barrier (BBB) model, comprised of porcine brain endothelial cells (PBECs) and primary rat astrocytes. Transduction was evaluated 10 days post addition of AAV9-NPC2-2A-GFP via expression of GFP detected by immunocytochemistry and RT-qPCR. The potential therapeutic effect of AAV9-NPC2-2A-GFP was investigated through ELISA for detection of secreted NPC2 protein. Potential detrimental effects were evaluated via transendothelial electrical resistance (TEER) measurements and immunostainings of Zona Occludens-1 (ZO-1) and GFAP.

Results: GFP was not detected in AAV9-NPC2-2A-GFP treated PBECs or astrocytes, and secreted NPC2 was lower than detection rate. TEER values were significantly lower in AAV9-treated barriers (n=9) compared to untreated (n=9) from days 1 through 5 after addition of AAV9-NPC2-2A-GFP ($p<0.05$), and astrocytes appeared more reactive by their GFAP-stainings. No differences were observed in ZO-1 stainings between treatment conditions.

Conclusion: AAV9-NPC2-2A-GFP could not transduce the in vitro BBB model, and NPC2 secretion could not be demonstrated. AAV9-NPC2-2A-GFP compromised barrier integrity of the BBB model.

Keywords: AAV9, NPC2, BBB models, gene therapy

Preface

The present thesis was conducted by Ida Køgs Andersen, Lissa Vestergaard Hauerslev and Lonnie Møller Johansen during 9th and 10th semester on Medicine with Industrial Specialization (Biomedicine) at Laboratory of Neurobiology (LNB), School of Medicine and Health, Aalborg University. The project, including all experimental work, was conducted from September 1st 2018 to May 31st 2019. Assistant professor Annette Burkhart Larsen and associate professor Louiza Bohn Thomsen provided supervision. The form of which the present project is presented is in agreement with our supervisor, Louiza Bohn Thomsen. Enclosed to the thesis are 8 appendices, in which supplementary data and -figures can be found. The Nature method was used for citation, and the bibliography includes all sources used. Finally, we would like to give our sincerest appreciation to supervisors Annette Burkhart Larsen and Louiza Bohn Thomsen, PhD student and co-supervisor Eva Hede Olsen, laboratory technician Hanne Krone Nielsen, and the remaining LNB group for being supportive throughout the project period.

Abbreviations

AAVs: Adeno-associated virus, **ABCA1:** ATP-binding cassette transporter A1, **ACAT**: Acyl-Coenzyme A cholesterol acyltransferase, **ACM**: Astrocyte conditioned media, **BBB**: Blood-brain barrier, **BECs**: Brain endothelial cells, **bFGF**: Basic fibroblast growth factor, **BSA**: Bovine serum albumin, **CNS**: Central nervous system, **EE**: Early endosome, **ER**: Endoplasmic reticulum, **FCS**: Fetal calf serum, **HBMEC**: Human brain microvascular endothelial cells, **HPRT1**: Hypoxanthine phosphoribosyltransferase 1, **HSV**: Herpes simplex virus, **ITR**: Inverted terminal repeats, **ITS**: Insulin-Transferrin-Selenium, **LDL**: Low density lipoproteins, **LDLR**: LDL-receptor, **LE**: Late endosomes, **LE/L**: Late endosomes/lysosomes, **LSOs**: Lipid storage organelles, **M6PR**: Mannose 6-phosphate receptor, **NPC1/2 disease**: Niemann Pick's type C1/2 disease, **NPC2 gene**: Niemann Pick's type C intracellular cholesterol transporter 2 gene,
NPC2 protein: Niemann Pick's type C intracellular cholesterol transporter 2 protein, **NC**: Nucleopore complex, **PBECs**: Porcine brain endothelial cells, **PDS**: Plasma derived bovine serum, **rAAV**: Recombinant adeno associated virus, **RE**: Relative expression, **RO**: Phosphodiesterase inhibitor RO-201724, **RT**: Room temperature, **SOC**: Super Optimal broth with Catabolite repression, **SREBP**: Sterol regulatory element binding protein, **$TCID_{50}$**: Median tissue culture infective dose, **TEER**: Trans-endothelial electrical resistance, **TGN**: Trans-Golgi network, **TJs**: Tight junctions, **vg**: Viral genomes, **WCE**: Woodchuck Hepatitis virus posttranscriptional regulatory element, **ZO-1/2**: Zonula Occludens 1/2

Table of contents

Addressing recombinant AAV9 as a novel therapeutic strategy for gene correction of Niemann Pick's type C2 disease in the CNS

1. Introduction

Niemann Pick's type C2 (NPC2) disease is a fatal disease caused by mutations in the NPC2 intracellular cholesterol transporter 2 gene (NPC2 gene). Current treatment is insufficient, and especially neurological symptoms are still severely affecting the quality of life of the patients suffering from NPC2 disease, as to why novel therapeutic strategies are needed. To treat the underlying cause of the disease, gene therapy may be considered, in order to secure production of functional NPC2 protein. The adeno associated virus serotype 9 (AAV9) is neurotropic after systemic injection, thus overcoming the blood-brain barrier (BBB), which is known to restrict many types of central nervous system (CNS) directed drug delivery strategies, hence why it could be a suitable candidate for gene correction within the CNS. The following will first elaborate upon the pathogenesis of NPC2 disease, after which the challenging BBB is presented, and then reasonings for utilizing AAV9 for gene correction of NPC2 disease.

1.1 Niemann Pick's type C disease

1.1.1 Clinical presentation

Niemann Pick's type C disease is a fatal autosomal recessive disorder caused by mutations in the NPC1 gene in 95% of cases or NPC2 gene in 5% of cases, resulting in deficiency of functional NPC1- or NPC2 proteins [1–3]. The combined incidence is 1 out of 89,000, and the incidence of NPC2 disease alone is 1 out of 2,900,000 [4]. Mutations in the NPC1 gene and NPC2 gene results in similar disease phenotypes [5], including both visceral and neurological symptoms such as prolonged neonatal jaundice, hepatosplenomegaly, ataxia, cognitive difficulties, dysphagia, dysarthria, cataplexy, and visual deterioration [6]. Age of onset varies from neonatal to adulthood, with an average around 6 to 8 years of age, and the age of death is highly dependent on the age of onset [6,7]. Age, clinical presentation and disease progression varies greatly between patients, making diagnosis difficult [6,7]. While NPC1- and NPC2 disease share an overlap in clinical presentation and pathogenesis, this paper will place an emphasis on NPC2.

1.1.2 Niemann Picks type C2

The NPC2 gene is located at chromosome 14q24.3, is 13,5 kb long, and contains 5 exons [8]. It codes for a soluble glycoprotein made out of 132 amino-acids [9]. The newly synthesized NPC2 protein is guided to the lysosomes via its mannose 6-phosphate tag interacting with mannose 6-phosphate receptors (M6PRs) located in the trans-Golgi network (TGN) [10,11]. However, some NPC2 proteins escape M6PRs in the TGN and are secreted from the cell [11,12]. When NPC2 protein is present in extracellular fluid, it is collected by cells via the M6PRs located at the cell surface and transported to the lysosomes [1,10]. The NPC2 protein is essential in the process of transporting cholesterol out of the late endosomes/lysosomes (LE/L) in cooperation with the NPC1 protein [5](*figure 1*). Thus, deficiency of NPC2 protein causes accumulation of cholesterol in the LE/L, creating abnormal lipid storage organelles (LSOs) [3,13], as depicted in detail in *figure 1*.

1.1.3 NPC2 protein deficiency and neurodegeneration

Though the mechanisms of functional NPC proteins in the systemic cell have been widely researched, the mechanisms linking NPC protein deficiency to the neurodegeneration observed in NPC patients are unknown [3]. However, increased autophagocytosis is observed to be linked to NPC1 deficiency [14,15], and to cholesterol starvation as a result of the cholesterol entrapment in LSOs [16]. Thus, it is reasonable to speculate that autophagy could be associated with NPC2 deficiency as well.

Interestingly, plasma lipoproteins cannot cross the BBB, which indicates that cholesterol in the CNS must be synthesized endogenously [17,18]. In the CNS, cholesterol is thought to be synthesized by glial cells, mainly astrocytes, and transported to neurons by lipoproteins containing apolipoprotein E [19,20]. Neurons take up these lipoproteins via receptors on their cell surface [21,22], and can extract their cholesterol cargo via the endosomal system [17], as illustrated in

figure 1. Because neurons do not produce sufficient cholesterol by de novo synthesis to supply their high demand, they are dependent on extracellular cholesterol supply [20,23]. Thus, neurons are severely affected by NPC2 deficiency, causing the endocytosed cholesterol to be trapped in LSOs [14], as depicted in *figure 1*. In addition, neurons affected by NPC protein deficiency will reduce proper axonal myelination, resulting in hypomyelination [24]. Oligodendrocytes, however, do not appear to accumulate cholesterol in LSOs [24,25]. It can be speculated whether this is due to their cholesterol need being satisfied by de novo synthesis, thus not depending on the endosomal pathway. Furthermore, it can be speculated whether the same pattern can be observed in other glial cells, e.g. astrocytes.

Indeed, mismanagement of cholesterol homeostasis in the CNS appears to be closely intertwined with neurodegeneration [19], however a deeper investigation into how lipid homeostasis correlates to neurodegeneration lies beyond this paper.

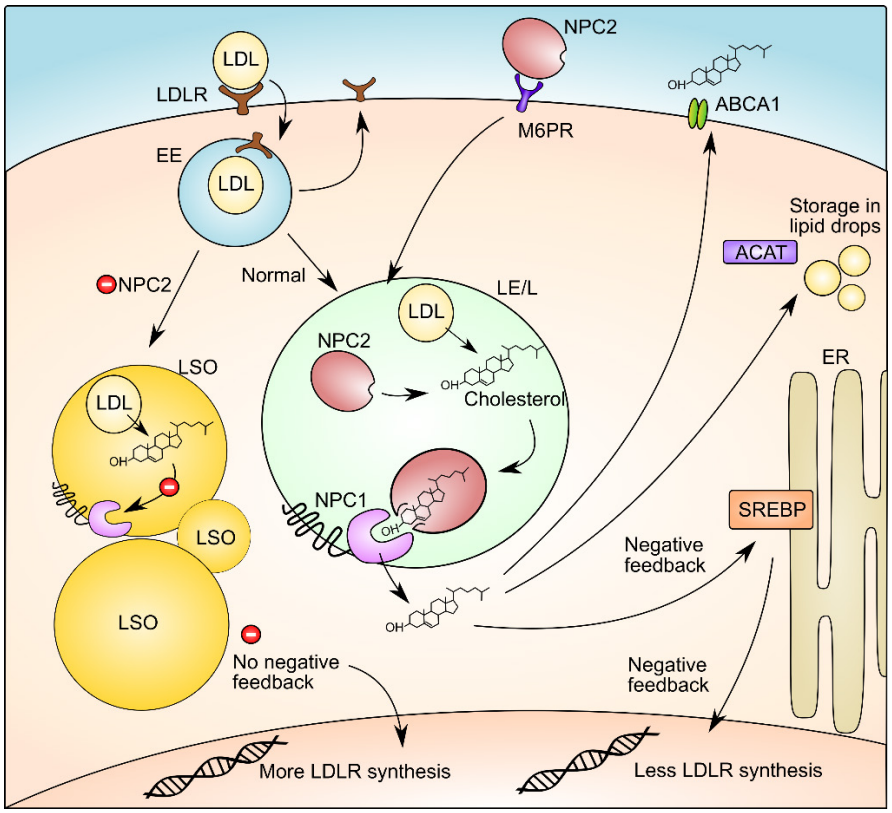

Figure 1: *Cholesterol handling in a normal cell and in a NPC2 protein deficient cell. Lipoproteins, e.g. low density lipoproteins (LDL), enter the cell by endocytosis via a LDL-receptor (LDLR) [17], creating an early endosome (EE) [12]. Later, the endosome merges with lysosomal proteins from the trans-Golgi network, creating the late endosome/lysosome (LE/L) [12]. Here, the cholesterol-esters are hydrolyzed to free cholesterol and transferred out of the LE/L via NPC1 and NPC2 [13]: The NPC2 protein is located in the lumen of the LE/L, arriving from in situ synthesis or from extracellular uptake via the mannose 6-phosphate receptors (M6PR) [1,10]. It binds the isooctyl side-chain end of cholesterol in a hydrophobic pocket with high affinity and the hydroxyl-end of cholesterol exposed [26]. This gives NPC2 the ability to transfer cholesterol from the lumen of the LE/L to NPC1 in the limiting membrane of the lysosomes [27]. Here, NPC2 interacts which NPC1 and facilitates opening of the cholesterol-binding pocket, and then transfers the cholesterol to NPC1 [27,28], which then is believed to transport the cholesterol out of the LE/L [17,29]. Because of the close interplay between NPC2 and NPC1 in transferring cholesterol out of the LE/L, deficiency of either one results in accumulation of cholesterol in the endosomal membranes, creating abnormal lysosomal lipid storage organelles (LSOs) [30]. Under normal conditions, free cholesterol will, after leaving the LE/L, be transported to the ER or to the plasma membrane [31], where cholesterol is vital for maintaining normal structure[32]. Excess of free cholesterol may leave the cells from the cell membrane mediated by the ATP-binding cassette transporter A1 (ABCA1), or it may undergo esterification by Acyl-Coenzyme A cholesterol acyltransferase (ACAT) to be stored intracellularly as lipid drops [12]. In the endoplasmic reticulum (ER), the sterol regulatory element binding protein (SREBP) strictly regulates the cellular cholesterol level by a negative feedback mechanism, which decreases the transcription factors responsible for expression of genes involved in cholesterol synthesis and LDL uptake [33]. When defects in NPC1 or NPC2 prevent export of cholesterol from the LE/L, the feedback mechanism to SREBP is thought to be lost, resulting in increased expression of genes involved in LDL uptake and cholesterol synthesis, further increasing cholesterol build-up [13]. Figure is created in Inkscape 0.92.*

1.1.4 Treatment of NPC

At present there is no cure for NPC disease [34,35]. Current management relies on symptomatic relief, often by administration of Miglustat, which is a reversible glucosylceramide synthase inhibitor [35–37]. Miglustat has been proven able to stabilize or delay the progression of irreversible neurological damage in NPC [34–36]. Unfortunately, a notable amount of patients still show deteriorating symptoms, despite treatment [34–36], which is especially true for patients with early onset of disease, compared to a later onset [34].

Because of the inadequacy of the current treatment, the severity of the disease and the great impact on quality of life, new treatments are needed. As Niemann Picks type C2 is caused by a mutation in the NPC2 gene, resulting in a dysfunctional NPC2 protein [1], an alternative strategy for disease management could be protein replacement therapy. This approach is supported by findings that NPC2 deficient cells can be cured from cholesterol mishandling by addition of medium conditioned by NPC2-transfected cells [1,38,39], thus indicating that NPC2 deficient cells can be cured by supplying replacement protein exogenously [1]. Another strategy for disease management may be to target the underlying cause of the disease by gene therapy, creating NPC2 protein secreting cells, hence supplying the protein indirectly. However, both strategies are challenging in regard to crossing the BBB, and as neurodegenerative symptoms constitute a large part of the pathologic manifestations of NPC2 disease, it is important to find a strategy which targets or passes the BBB, making sure the treatment can address the neurological symptoms.

1.2 The blood brain barrier

The BBB is a neuroprotective barrier, separating the circulating blood from the CNS [40,41]. The barrier consists of non-fenestrated brain endothelial cells (BECs), joined together by junctional complexes, in close association with astrocytes and pericytes [41–44]. An essential component of the junctional complexes is tight junctions (TJs), which are responsible for the tightness of the barrier [41,44,45]. The TJs consist of proteins such as Occludin and Claudins, as well as junctional adhesion molecules, which span across the intercellular cleft [40,42,46]. Furthermore, Occludin and Claudins are linked to scaffolding and regulatory proteins, such as Zonula Occludens 1 (ZO-1) and ZO-2 [40,42,46]. The construction of the TJs prevents free diffusion across the barrier, thereby blocking the passage of macro- and hydrophilic molecules, including NPC2 proteins, only allowing small gaseous- or lipophilic molecules to pass the BBB [41,44,45]. This has posed a notorious limitation in designing therapies for the CNS via non-invasive routes.

Many essential nutrients necessary for the metabolism in nervous tissue are hydrophilic molecules, such as glucose and amino acids, which cannot passively cross the barrier [40,41,44,45]. To accommodate this requirement, the BBB contains specific transport systems, which ensure a controlled blood-brain exchange of these nutrients [40,45,47]. Likewise, the BBB expresses transporters which clear out potentially neurotoxic molecules from the brain, thereby protecting and detoxifying the CNS [40,45]. While this mechanism is beneficial for the healthy brain, it adds to the complexity of CNS-directed therapy, as therapeutic molecules may be effluxed via transporters such as members of the ATP-binding cassette transporter family [42,45]. The combination of restricted permeability and efflux transporters has posed a challenge in treating CNS symptoms, but may be overcome by gene therapy.

1.3 Gene therapy

Gene therapy targeting the CNS often relies on invasive methods, such as administration of the vector directly into the brain parenchyma. However, with the appropriate vector it may be possible to surpass the BBB, such that less invasive methods can be employed, i.e. intravenous administration [48,49].

If this is achieved, it may be an ideal therapeutic approach for lysosomal storage diseases such as NPC, as it would be possible to target the underlying genetic cause of disease, hence eliminating the need for chronic administration of conventional symptom management therapy [37]. For chronic diseases such as NPC2, stable gene transduction is more desirable, negating the need for frequent administration. For this reason, viral gene therapy may be preferable compared to non-viral, because, despite advancements in non-viral gene therapy, viral gene therapy is generally superior in terms of sustained gene expression [50].

1.3.1 Viral vectors for gene-correction of CNS disorders

The use of several viral vectors has already been attempted for treatment of CNS disorders [48,51], e.g. herpes simplex virus (HSV), lentivirus, and adenovirus.

HSV vectors have some innate advantages when it comes to gene therapy targeting the CNS, as they have a natural tropism towards neurons, and can efficiently transduce them in vivo [52]. Their ability for anterograde and retrograde

transport [53] may also provide a benefit in terms of distributing the gene therapy throughout the CNS. However, depending on HSV vector type, they may be difficult to generate, and may yield a very low titer [54]. While most classes of retrovirus are not favorable, lentiviral vectors may be an exception, as they can mediate transgene expression in dividing as well as non-dividing cells [48]. They have been shown to elicit efficient neuronal expression in rodents [55,56], but are associated with a substantial limitation in terms of drug-delivery, as their volumetric spread into the parenchyma extends to only 500-700 µm from the injection site [57]. Unfortunately, retrovirus also generally pose a substantial safety concern due to pro-viral integration into the host genome with a risk for viral integration into proto-oncogenes [58]. Lentivirus are less oncogenic than other retrovira [59], but the risk should not be negated. Adenoviral vectors have some advantages, as the transgene remains episomal[48], while still delivering stable, sustained gene expression [60], and the large packaging capacity (36 kb) [61] puts fewer limitations on the transgene construct. Furthermore, a transduction of a wide range of CNS cell populations is obtainable after direct infusion [62,63]. Unfortunately, the Ad capsid is highly immunogenic [64], negating the benefits of the vector.

Because of the relative disadvantages to the above-mentioned vectors, AAVs may be advantageous for gene therapy of NPC2 disease.

1.3.2 Adeno-associated virus

AAVs are small (~18-26 nm), non-enveloped virus [65] belonging to the Dependoparvovirus genus of the Parvoviridae family. They are reliant on co-infection with a helper virus in order to replicate [66], and a wild type infection is thus far not known to cause disease [67], which makes AAVs a safer alternative compared to HSV, retro- and adenovirus. In addition, AAVs are believed to be less immunogenic than e.g. adenovirus [64,68], and innovative recombinant AAVs (rAAVs) may be a way to overcome or limit the immunogenicity [69]. Despite a risk of viral integration into the host genome [70–73], it is largely agreed that the AAV genome predominantly remains episomal [73,74]. Furthermore, integration has not yet been reported in humans [67] and may therefore be safer compared e.g. to lentivirus. Moreover, AAVs are capable of transducing dividing and non-dividing cells [48], and have been reported to be able to elicit long-term gene correction in the human brain [68].

The natural serotypes of AAVs have been found to distribute widely in human tissues [75], providing rationale for choosing such a capsid for treatment of a genetic disorder with widespread dissemination such as NPC [6]. This study focuses on AAV9, using a wild type capsid for production of rAAV9. AAV9 based gene therapy is already in clinical trials for other disorders affecting the CNS, e.g. for late-onset Pompe's Disease [76] and Spinal Muscular Atrophy Type 1 [77]. Hence, AAV9-based gene therapy appears to be a promising field, and seems suitable for NPC2 disease, because of the tissue distribution profile (widespread distribution, liver involvement, CNS involvement). Furthermore, animal studies on NPC1 disease using AAV9 gene therapy have shown improved symptoms, increased lifespan and decreased neuronal cell death [78,79], supporting the likelihood that similar improvements may be observed in NPC2 disease. AAV9 is chosen over other serotypes, because it is a unique human serotype able to transduce cells of the CNS with intravenous administration [51], negating the need for invasive administration methods. The mechanism with which it enters the CNS is believed to be transcytosis, via an active process which has been found not to affect the integrity of a human BBB [80]. This is important, because as mentioned previously, the BBB also ensures CNS protection from pathogens and toxins, and an increased permeability would impair this.

A therapeutic effect using rAAVs can only be achieved if certain molecular interactions take place between the virus and host cell at every step of its infectious path. First, viral entry into the host cell depends on receptor/coreceptor-attachment to the cell membrane with subsequent endocytosis [81]. The molecular basis for this is determined by its capsid structure; in fact, serotypes are divided based on their phylogenetic similarities in capsid sequence [75]. AAVs are encapsidated by 60 copies of an assemblage of capsid proteins. Each copy consists of three structural proteins, VP1, VP2 and VP3, which are clustered in a 1:1:10 ratio, collectively forming an icosahedral virion structure [82–84]. Each of the proteins participate in the successful transduction of a target cell as elaborated upon in *figure 2*.

A possible limitation to the therapeutic potential of AAV9 is the limited coding capacity (~4.7 kb single stranded genome) [85], but it may not be an obstacle in treating Niemann-Pick Disease type C2 due to the relatively limited size of the NPC2 gene, which can be delivered as cDNA comprising only 1446 bp [86]. However, the limited coding capacity puts constraints on the design of the transgene. One way of optimizing the gene therapy with its limited capacity, is choice of promoter upstream of the NPC2 transgene. For instance, more cell specific promoters can be selected to increase transcription in target cells, and avoid or limit transcription of the transgene in cell populations considered off-target [87–89]. However, constitutive CAG and CMV promoters, whose transcriptional activity have been found to vary

with cell type [90], are amongst some of the more commonly used promoters for CNS-directed gene therapy using AAVs [91].

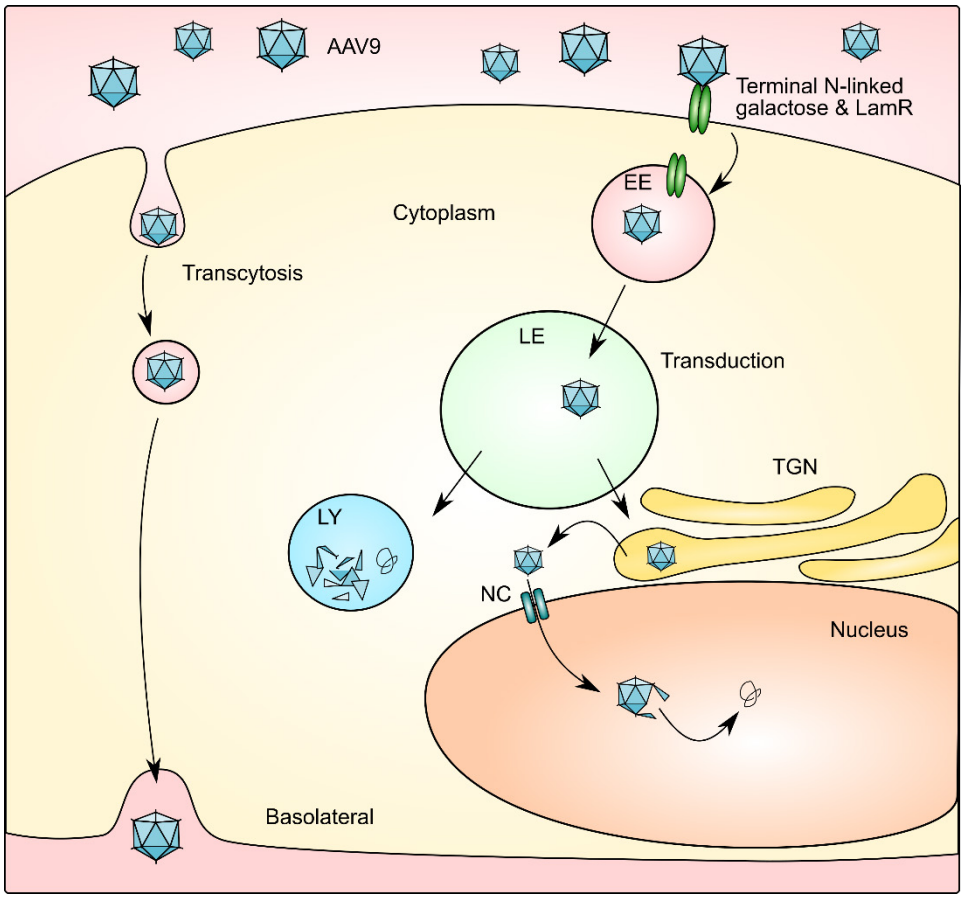

Figure 2: *Receptor binding and intracellular transport of AAVs. AAVs binds to a receptor/co-receptor complex, which for AAV9 is the terminal N-linked galactose [92,93] and LamR [51]. The icosahedral AAV capsid consists of a cluster of three proteins; VP1, VP2 and VP3. The VP3 protein has a core comprised of a β-barrel motif with interstrand loops. These interstrand loops are variable between serotypes and determine the molecular interactions with target cell receptors [94], hence its structure is crucial in the first step of the virion-target cell interaction. The binding elicits endocytosis of the virion, followed by retrograde transport via first the early endosomes (EE), then late endosomes (LE). From hereon, they may be degraded in lysosomes or reach the trans-Golgi network (TGN). VP1 has been implicated in the escape of the virion from endosomes via its phospholipase A2-domain [95,96], which is exposed by capsid conformation changes [81]. VP2 may support infectivity, e.g. VP1 may rely on VP2 for subsequent release from the Golgi or endoplasmic reticulum (ER), transport to the nuclear membrane and import through the nucleopore complex (NC) [81,95–97]. After nuclear import, virions are uncoated, releasing their genome in the nucleoplasm. AAV genomes can be found in different molecular states after entering the nucleus, but are commonly found as double-stranded circular episomes [73]. Though the above is assumed to be applicable for AAV9, the majority of research has been conducted on the AAV2 serotype [81], hence some details may vary for each serotype. Furthermore, some of the steps remain poorly elucidated [81]. Another outcome following viral entry through the apical membrane is transport to the basolateral side via transcytosis. AAV9 in particular may cross brain capillary endothelial cells through transcytosis [80]. Figure is made in Inkscape 0.92.*

1.4 In vitro evaluation of CNS-directed gene therapy

To evaluate AAV9 as a novel gene therapy for NPC2 disease, initial in vitro testing of the vector is essential, which may initially be evaluated in in vitro BBB models. Several variations of in vitro BBB models have been developed, as they are more ethically acceptable, and can be more easily controlled than in vivo studies. These models have been constructed with immortalized cells, such as bEnd.3 and cEND, as well as with primary cells [43,47,98,99], which are typically of rodent, porcine and even human origin [99–103]. The models are based on primary BECs in either co- or triple-culture with primary astrocytes and -pericytes [99,104]. Co-culturing with astrocytes and pericytes in vitro has been found to be important for proper barrier function [42,45,46,99]. Though the interaction between astrocytes, pericytes and BECs are not fully understood, co-culturing leads to tighter TJs as well as induction of other BBB properties, making the BBB

less leaky [41,42,99,105]. This is considered to be partly caused by secretion of a range of molecules from the astrocytes and pericytes, such as basic fibroblast growth factor (bFGF), angiopoietin 1 and transforming growth factor-β [46,99,105]. In addition to co-culturing the BECs with astrocytes and pericytes, it has also been found that supplementing with hydrocortisone and phosphodiesterase inhibitor RO-201724 (RO), as well as increasing the intracellular cAMP in the BECs, strengthen the BBB properties [41,99,106–108].

To evaluate the barrier function of in vitro BBB models, trans-endothelial electrical resistance (TEER) is often used as a marker of tightness, and radiolabeled mannitol assays are used to assess passive permeability [46,99]. Studies have found a correlation between TEER and permeability assays in in vitro barrier models, showing that a high TEER also entails low permeability, and likewise that low TEER entails high permeability of the barrier [99,108]. As TEER measurements are less invasive than radiolabeled mannitol permeability assays, and because of the correlation between them, TEER measurements may be used as a general non-invasive marker of barrier integrity in in vitro BBBs [109].

1.5 Aim of study

This study aimed to produce AAV9 vectors expressing NPC2-2A-GFP, for the purpose of evaluating it as a novel therapeutic strategy in treatment of NPC2 disease.

The hypothesis of this study was that AAV9-NPC2-2A-GFP could transduce in vitro BBB models and induce NPC2 protein secretion, without compromising the BBB integrity.

This hypothesis was tested by treating in vitro non-contact BBB models, comprised of porcine brain endothelial cells (PBECs) and primary rat astrocytes with the AAV9-NPC2-2A-GFP. Transduction was evaluated via expression of the transgenic GFP detected by ICC and RT-qPCR. The potential therapeutic effect of the AAV9-NPC2-2A-GFP was investigated through ELISA for detection of secreted NPC2 protein on the conditioned media from the BBB models, and the BBB integrity was monitored via TEER measurements and qPCR on TJ proteins.

In addition, it was hypothesized that choice of promoter could modulate transgene expression. To investigate this, CAG- and CMV promoters were evaluated for their potential to modulate transgene expression. Furthermore, a luciferase assay was evaluated for its benefits and shortcomings in evaluation of transfection efficiency.

2. Methods

2.1 Cell culture

2.1.1 Cell lines

HeLa cells were maintained in RPMI 1640 GlutaMAX™ (1X, cat. #61870-010, Gibco, Life Technologies™) supplemented with 10% fetal calf serum (FCS) (cat. # 10270106, Gibco™) and 25 µg/mL gentamicin (cat. #17-518Z, Lonza).

HEK293FT cells were maintained in high glucose DMEM GlutaMAX™ (1X, cat. #31966-021, Gibco, LifeTechnologies™) supplemented with 10% FCS and non-essential amino acids (1X, cat. #11140050, Gibco™). Human brain microvascular endothelial cells (HBMEC), isolated from a brain biopsy of an adult female with epilepsy and immortalized by Greiffenberg et al.[110], and bEnd.3 cells were maintained in high glucose DMEM GlutaMAX™ (1X) supplemented with 10% FCS, L-glutamine (4 mM, cat. #G7513, Sigma-Aldrich), 25 µg/mL gentamicin, and 10 ng/mL bFGF (cat. #13256-029, Gibco™).

RBE4 cells were maintained in high glucose DMEM GlutaMAX™ (1X) supplemented with 10% FCS, 4 mM L-glutamine, 25 µg/mL gentamicin, 300 µg/mL geneticin (G418) (cat. #G8168, Sigma), and 10 ng/mL bFGF.

All medium was sterile filtered before use. All cell types were maintained in plastic flasks (cat. #660175, cat. #658175, Greiner CELLSTAR ®) at 37 °C, 20 % O_2, and 5 % CO_2.

2.1.2 Primary cells

Primary rat astrocytes, kindly provided by Annette Burkhart Larsen [111], had been isolated from 2-day old Sprague-Dawley rats according to procedures previously described, and was approved by the Danish National Council of Animal Welfare [111]. They were maintained in low glucose DMEM GlutaMAX™ (1X, cat. #21885025, Thermo Fisher) supplemented with 10% FCS and 10 µg/mL gentamicin.

PBECs were kindly provided by Louiza Bohn Thomsen [99]. They had been isolated from 6 month old domestic pig brains according to procedures previously described [99]. As the brains were obtained from an abattoir (Danish Crown, DK), the animals were handled and euthanized according to legislation issued by the Danish and European Food Standard Agency, and as such, no additional ethical approval was needed for isolation of PBECs [99]. PBECs were maintained in DMEM/F12 (cat. #31331-028, Gibco™) supplemented with 10% plasma derived bovine serum (PDS) (First Link Ldt), 1% Insulin-Transferrin-Selenium (ITS) (cat. #11074547001, Roche), 10 µg/mL gentamicin and 1 ng/mL bFGF.

All medium was sterile filtered before use, and cells were maintained at 37 °C, 20 % O_2, and 5 % CO_2.

2.2 Production and purification of AAV9 vectors

An AAV9-NPC2-GFP vector was produced with the purpose of investigating the potential of AAV9 as a novel therapeutic strategy in in vitro BBB models. The production of AAV9-NPC2-2A-GFP was performed by triple transfection of a packaging cell line, HEK293FT, expressing adenoviral E1a/E1b genes [112]. HEK293FT cells were transfected with helper plasmid pAdDeltaF6 containing helper genes E4, E2a and VA, pAAV9 encoding rep/cap genes, and pFastbac-CAG-NPC2-2A-GFP containing the gene of interest and a fluorescent protein flanked by inverted terminal repeats (ITR).

2.2.1 Amplification of helper- and rep/cap plasmids

Prior to AAV9 production, helper plasmid pAdDeltaF6[113], and *rep/cap* plasmid pAAV9, both provided by Eva Hede Olsen (Laboratory of Neurobiology, Aalborg University), were amplified by transformation of chemically competent E. coli (Subcloning Efficiency™ DH5α™ Competent E. coli, cat. #18265-017, Invitrogen™). For each type of plasmid, 10 ng plasmid DNA was mixed with 50 µL chemically competent E. coli and incubated for 30 min on ice. Following incubation, the reactions were heated to 42°C for 20 s in a water bath, and subsequently put on ice for 2 min. Next, 450 µL Super Optimal broth with Catabolite repression (SOC) media (cat. #15544-034, Invitrogen) was added to each reaction and they were incubated for 1 h at 37°C and 200 RPM on an orbital shaker (KS 501 digital orbital shaker, IKA™). The bacterial suspension was then spread onto LB agar plates (Luria Bertani, cat. #L2897-1KG, Sigma-Aldrich) containing 100 µg/mL ampicillin sodium salt (cat. #A9518-5G, Sigma-Aldrich), and stored at 37°C overnight.

The following day, bacterial colonies were transferred from agar plates to sterile flasks containing LB medium (LB Broth (Miller), (cat. #L3522-1KG, Sigma-Aldrich) with 100 µg/mL ampicillin and incubated overnight at 37°C and 250 RPM.

2.2.2 Amplification of transgene plasmid

pFastbac-CAG-NPC2-2A-GFP was provided by Eva Hede Olsen (Laboratory of Neurobiology, Aalborg University), and was amplified using a modified protocol, taking the fragile ITR-regions into consideration. This protocol follows the same procedures as described in *section 2.2.1*, but with incubation of bacteria at no more than 30°C and at no more than 175 RPM in a Forma Scientific Incubated benchtop Orbital Shaker (Forma™, Thermo Scientific™).

2.2.3 Plasmid purification and precipitation

Plasmids were purified using a Nucleobond® Xtra Midi EF kit (cat. #740410.10, Macherey-Nagel) according to manufacturer's protocol for high-copy plasmid purification. Bacterial cells were pelleted by centrifugation at 4,500 g for 10 min at 4°C, after which the supernatant was discarded, and the pellet was resuspended in Buffer RES-EF containing RNase A. Cells were lysed by addition of Buffer LYS-EF, followed by 5 min of incubation at room temperature (RT). The lysate was neutralized by addition of Buffer NEU-EF, and the suspension was loaded into Nucleobond® Xtra Midi Column filters, placed in Nucleobond® Xtra Midi Columns, which had been pre-wet with Buffer EQU-EF. The columns were allowed to empty by gravity flow, after which the filters were washed with Buffer FIL-EF, and the filters were discarded. Next, the columns were washed with Buffer ENDO-EF, followed by a wash with Buffer WASH-EF. Finally, the plasmid DNA was eluted by addition of Buffer ELU-EF and collected in centrifuge tubes. The plasmid DNA was precipitated by addition of isopropanol, followed by centrifugation at 7,000 g for 15 min. The supernatant was discarded, and 70% ethanol was added to the pellet, followed by centrifugation at 7,000 g for 5 min. Lastly, the ethanol was removed, and the pellet was redissolved in Buffer TE-EF.

The plasmid purification was followed by DNA precipitation by addition of a polyethylene solution containing 12.5 % PEG 6000 (cat. #25322-68-3, Merck) and 3.75 % NaCl (cat. #27810.295, VWR™), and was then incubated on ice for 30 min. Next, the precipitate was centrifuged at 7,000 g and 4°C for 15 min, and the supernatant discarded. The precipitate was then washed with 70% ethanol, and centrifuged at 11,000 g and 4°C for 5 min. After centrifugation, ethanol was removed before the pellet was resuspended in TE buffer (cat. #8019005, Invitrogen), and dissolved by heating it in a lukewarm water bath.

Plasmid concentrations were measured on a spectrophotometer (Nanodrop™ ND-1000 spectrophotometer, Thermo Scientific™), and the plasmids were kept at -20°C until use.

2.2.4 Plasmid sequence verification

The plasmids were verified by restriction analysis. pFastbac-CAG-NPC2-2A-GFP was digested by mixing DNA (25 ng/µL) with FastDigest (FD) Green Buffer (1X, cat. #B72, Thermo Scientific™) and FD XhoI (1X, cat. #FD0694, Thermo Scientific™) in nuclease-free water. Intact ITR-regions of pFastbac-CAG-NPC2-2A-GFP was verified by digestion of DNA (25 ng/µL) with FD SmaI (1X, cat. #FD0663, Thermo Scientific™) in FD Green Buffer (1X) and nuclease-free water. A double digest was used for pADdeltaF6 (25 ng/µL) with FD BamHI (1X, cat. #FD0054, Thermo Scientific™) and FD NdeI (1X, cat. #FD0583, Thermo Scientific™) in FD Green Buffer (1X) and nuclease-free water. All reactions were heated in a heating block (Eppendorf ThermoMixer® F1.5) at 37°C for 10 min. The restrictions digests were analysed by gel electrophoresis (RunOne™ system, Embitec™) in an agarose gel (1 % agarose, cat. #BN-50004, BioNordika in Tris-acetate-EDTA) supplemented with GelRed™ (1 X, cat. #41003, Biotium). DNA bands were measured via an Odyssey Fc Infrared Imaging System (Li-Cor) and were compared to a 1 kilobase ladder (cat. #SM0313, Thermo Scientific™).

pFastbac-CAG-NPC2-2A-GFP and pAdDeltaF6 corresponded well to their sequence. pAAV9 could not be verified by restriction analysis, as the sequence of this provided plasmid was unknown.

2.2.5 Transfection of HEK293FT cells

24 h before transfection, HEK293FT cells were seeded in 145 mm cell culture dishes (cat. #639160, Greiner Bio-One) to a confluency of approximately 50-70% on the day of transfection. A transfection solution was prepared: per dish, 12 µg DNA (pADdeltaF6, pAAV9, and pFastbac-AAV-CAG-NPC2-2A-GFP in a ratio of 2:1:1) was dissolved in high glucose DMEM (1X) to a total volume of 450 µL, after which 120 µL Polyfect Transfection Agent (cat. #301107, Qiagen) was added. The solution was mixed well and incubated for 10-15 min at RT to allow complex formation. Following incubation, standard HEK293FT cell medium was added to the transfection solution (*see section 2.1.1*), and the solution was distributed dropwise to the cell cultures, and mixed by swirling them gently. Media was changed to fresh standard HEK293FT cell medium after 24 h to remove the transfection solution.

2.2.6 Harvest and purification

The cells were kept in culture for a total of 96 h after transfection, after which the cell culture medium and transfected HEK293FT cells were harvested and purified as illustrated in *figure 3*.

The harvested cells and cell culture medium was pooled into centrifuge tubes and centrifuged for 5 min. at 250 g and 4°C. The cell culture supernatant was then aspirated and transferred to new centrifuge tubes. The cell pellet was resuspended in sterile filtered 10X PBS supplemented with 10 mM $MgCl_2$ (cat. #M8266, Sigma Aldrich) and 25 mM KCl (cat. #1.04936, Merck) (PBS-MK). The cell pellet suspension was then put through three freeze/thaw cycles in which they were kept at -80°C until frozen, and thawed in a 37°C water bath to release intracellular viral genomes (vg).

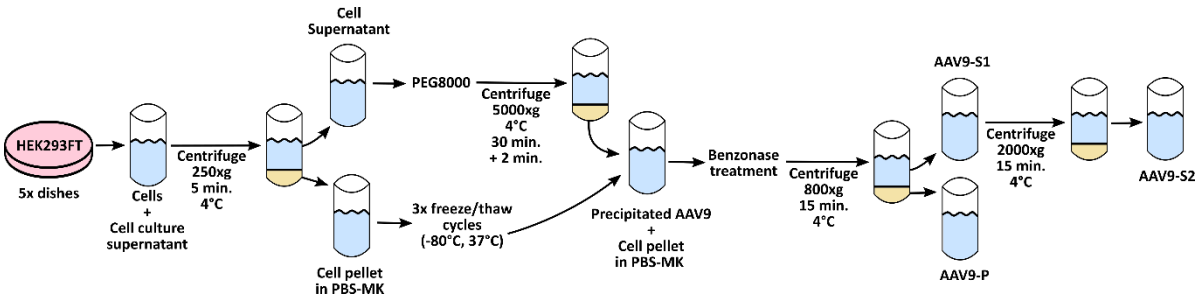

***Figure 3**: Overview of purification procedure of AAV9-NPC2-2A-GFP-P, AAV9-NPC2-2A-GFP-S1 and AAV9-NPC2-2A-GFP-S2.*

The AAV9-NPC2-2A-GFP in the cell culture supernatant was precipitated by addition of 0.1 g/mL PEG 8000 (cat. # P4463, Sigma Aldrich) and 0.058 g/mL NaCl, after which it was stored at 4°C overnight in a Tube Rotator (cat. #88881002, Thermo Scientific™) for proper dissolving. Afterwards, the PEG 8000/NaCl solution containing the precipitated virus were centrifuged at 5,000 g and 4°C for 30 min, after which the supernatant was discarded immediately. This was followed by an additional centrifugation step at 5,000 g and 4°C for 2 min and a subsequent complete removal of the remaining supernatant with a pipette. The precipitated AAV9-NPC2-2A-GFP from the cell culture supernatant was then resuspended in 1 mL PBS-MK and pooled with the cell lysate. Benzonase® nuclease (cat. #E1014-5KU, Sigma-Aldrich) was added to the pooled viral solution in a concentration of 50 U/ml and incubated in a 37°C water bath for 30 min, after which it was centrifuged at 800 g and 4°C for 15 min to remove cellular debris. The pellet of cell debris was resuspended in 1 mL PBS-MK and kept for later analysis. Throughout the study, this will be referred to as "AAV9-NPC2-2A-GFP-P" (*table 1*). Half of the supernatant underwent an additional centrifugation at 2000 g for 15 min. at 4°C, after which both supernatant samples were kept for later analysis. Throughout the study, these will be referred to as "AAV9-NPC2-2A-GFP-S1" and "AAV9-NPC2-2A-GFP-S2" (*table 1*). All samples were kept for no longer than a week at 4°C, after which they were transferred to -80°C.

Abbreviation	**Description**
AAV9-NPC2-2A-GFP	AAV9-NPC2-2A-GFP provided by our laboratory, purified by iodixanol gradient centrifugation
AAV9-NPC2-2A-GFP-P	Pellet from the AAV9-NPC2-2A-GFP production described in *section 2.2.*
AAV9-NPC2-2A-GFP-S1	Supernatant from the AAV9-NPC2-2A-GFP production described in *section 2.2.*
AAV9-NPC2-2A-GFP-S2	Supernatant after additional centrifugation of AAV9-NPC2-2A-GFP-S1 as described in *section 2.2.*

Table 1: Overview of the AAV9-NPC2-2A-GFP vectors used in this study

2.2.7 Virus titration

An absolute qPCR was performed to evaluate the titer of the AAV9-NPC2-2A-GFP-P, AAV9-NPC2-2A-GFP-S1 and AAV9-NPC2-2A-GFP-S2 samples, as well as provide information on how the vg were distributed between the three samples.

Primers were designed to amplify the CAG sequence within the recombinant viral genome (primer sequences are illustrated in *table 2*). A standard was made on serial 10-fold dilutions of a plasmid containing CAG, with a known stock concentration of 5x10^6 CAG-fragments/µL, provided by our laboratory. AAV9-NPC2-2A-GFP-P and AAV9-NPC2-2A-GFP-S1 samples were run in dilutions of 100, 1,000, 10,000 and 100,000 for further evaluation of the concentrations, while AAV9-NPC2-2A-GFP-S2 was run in dilutions of 1,000 and 10,000. For the PCR reaction, samples and standard were loaded in duplicates in a 96-well plate (cat. #AB2396 clear, Thermo Scientific™), along with SYBR Green (1X, cat.# K0251, Thermo Scientific™) with ROX passive reference dye, 5 µM forward primer and 5 µM reverse primer in nuclease-free water.

CAG Forward primer	AAC CCC AAT AGG GAC TTT C
CAG Reverse primer	GTA GGA AAG TCC CAT AAG GTC A

Table 2: Forward and reverse primers for amplification of the CAG sequence in AAV9-NPC2-2A-GFP titration. Primers were ordered from TAG Copenhagen.

The PCR reaction was run in a AriaMx Real-Time PCR system (Agilent Technologies), with an initial denaturation step at 95°C for 10 min, followed by a 3-step protocol with 40 cycles of denaturation at 95°C for 30 s, annealing at 62 °C for 30 s, and extension at 72°C for 30 s. Finally, a melting curve analysis was run at 95°C for 30 s, followed by 30 s at 62°C, and 30 s at 95°C with a resolution of 0.5°C and soak time of 5 s.

Analysis was performed in the Agilent Aria 1.5 software, and statistical analysis was performed in Excel 2016, in which the dilutions were accommodated for by multiplying with each respectable dilution factor. Data is illustrated by use of GraphPad Prism 6. Samples with a melting temperature (Tm) different from 81 were excluded from the data due to nonspecific product amplification (*see appendix 1.1 for melting curves and appendix 1.2 for exclusion criteria*).

2.2.8 Evaluation of AAV9-NPC2-2A-GFP-P/S2 by immunocytochemistry (ICC) of transduced primary rat astrocytes

ICC was performed on transduced primary rat astrocytes to evaluate the infectivity of AAV9-NPC2-2A-GFP-P and AAV9-NPC2-2A-GFP-S2, and to investigate whether they are able to express their transgene.

Prior to transduction, astrocytes were maintained as described in *section 2.1.2*, seeded on poly-L-lysine (5 µg/mL, cat. #P6282, Sigma Aldrich) coated coverslips in 24-well plates (cat. #662160, Greiner CELLSTAR®), and cultured until confluent. The cells were transduced by addition of AAV9-NPC2-2A-GFP-P and AAV9-NPC2-2A-GFP-S2 (*table 1*), respectively, to their culture medium, followed by a gentle stirring of the plates. AAV9-NPC2-2A-GFP-P was added in a concentration of $8.3x10^9$ vg per well, while AAV9-NPC2-2A-GFP-S2 was added in a concentration of $1.1x10^9$ vg per well, based on the titer results in *section 3.1.1* (*figure 6*). The cells were transduced for 24 h, after which media was changed. They were cultured for 10 days following transduction, with a bi-weekly media change.

Prior to ICC, the cells were washed twice in PBS, fixated with 4% paraformaldehyde (cat. #100496, Merck™) for 10 min at RT, after which they were washed another two times in PBS. Then, cells were permeabilized and blocked for 30 min with a blocking buffer consisting of 3% bovine serum albumin (BSA) (Cat. #EQBAH62-1000, Europa Bioproducts Ltd) and 0.2% Triton X-100 (cat. #X100-100ML, Sigma-Aldrich) in 1X K-PBS. Next, the astrocytes were stained with Rabbit anti-GFP (1:2,000 in blocking buffer, cat. #ab6556, Abcam) to enhance detection of transduced cells, and Mouse anti-GFAP (1:500 in blocking buffer, cat. #MAB360, Millipore) was used as an astrocyte marker. The antibodies were added to their respective wells, and incubated for 1 h at RT. After incubation, the wells were washed two times for 5 min in a washing buffer, consisting of blocking buffer in 1X K-PBS (1:50). Goat anti-rabbit Alexa Fluor 488-conjugated secondary antibodies (1:500 in blocking buffer, cat. #A11008, Invitrogen) were added to wells with anti-GFP, and Goat anti-mouse Alexa Fluor 594-conjugated secondary antibodies (1:500 in blocking buffer, cat. #A11032, Invitrogen) were added to wells with anti-GFAP. All wells were then incubated for 1 h at RT. Afterwards, the wells were washed for 5 min in 1X K-PBS. Nuclei were then counterstained with DAPI (1 µg/mL in 1X K-PBS, cat. #D9542, Sigma-Aldrich) for 4 min, after which the cells were washed two times in 1X K-PBS.

All incubation steps were performed while on a Belly Dancer® shaker (Stovall Life Science), protected from light. Non-transfected astrocytes were used as controls for non-specific binding. The coverslips were mounted on glass slides with DAKO fluorescent mounting media (cat. #S3023, Dako), and the cells were examined in an Axio Observer Z1 fluorescence microscope, equipped with ApoTome and Axiocam MR camera. Images were processed in ImageJ (v1.52i) and inkscape (0.92.3).

2.3 Effects of AAV9-NPC2-2A-GFP on HeLa cells

Due to impurity and low concentrations of the produced virus (AAV9-NPC2-2A-GFP-P, AAV9-NPC2-2A-GFP-S1 and AAV9-NPC2-2A-GFP-S2), further investigation of the potential of AAV9-NPC2-2A-GFP treatment was done with a vector provided by our laboratory. The provided AAV9-NPC2-2A-GFP was produced based on the same protocol described in *sections 2.2.5* and *2.2.6*, but with an additional purification step by iodixanol gradient ultracentrifugation. Before in vitro BBB studies, the infectivity of AAV9-NPC2-2A-GFP was investigated in HeLa cells. Prior to transduction, the HeLa cells were seeded into 24-well plates with and without coverslips in a density of 18,000 cells per cm^2, and maintained as described in *section 2.1.1*. 24 h after seeding, the medium was changed to fresh standard medium, and the HeLa cells were transduced by addition of $4x10^9$ vg per well. After addition of the vg, the plates were gently stirred to distribute them evenly within the wells. The cells were transduced for 48 h before harvesting for ICC and flow cytometry.

2.3.1 ICC on AAV9-NPC2-2A-GFP transduced HeLa cells

Cells were fixed, and ICC was performed on AAV9-NPC2-2A-GFP transduced HeLa cells and untreated controls similarly to the description in *section 2.2.8*. Rabbit anti-GFP was used to enhance detection of transduced cells with addition of Goat anti-rabbit Alexa Fluor 488-conjugated secondary antibodies.

2.3.2 Flow cytometry on AAV9-NPC2-2A-GFP transduced HeLa cells

For flow cytometry, the cells were washed two times in 1X PBS, after which they were trypsinized with trypsin-EDTA (0.25 %, Gibco™, cat. #15090046). When the cells had disassociated from the wells, the trypsinization was stopped by addition of HeLa standard medium, and the cells were transferred to centrifuge tubes, pooling two wells into one sample. The cells were then centrifuged at 300 g for 5 min at 4 °C, the medium was removed and 1X PBS was added to the tubes. The tubes were then vortexed for a second, and the centrifugation was repeated. After centrifugation, PBS was removed and the cells were resuspended in fresh PBS for flow cytometry analysis. The samples were kept on ice and protected from light until analysis.

Samples were analyzed on a CytoFLEX S Flow Cytometer (model #B75442, Beckman Coulter), using a 488-nm laser and FITC channel for detection of the GFP-tag. Acquisition settings for forward scatter was set to 61, side scatter was set to 37 and FITC was set to 70. For each sample, 20,000 events were recorded.

Data was processed in CytExpert version 2.3, in which each sample was manually gated. Untreated cells were used as negative controls to correct for auto-fluorescence, allowing a false positive rate of 0.5%.

2.4 Effects of AAV9-NPC2-2A-GFP on primary astrocytes

Prior to in vitro BBB studies, the effects of the provided AAV9-NPC2-2A-GFP was investigated by transduction of primary astrocytes in monoculture. Prior to transduction, astrocytes were maintained as described in *section 2.1.2*, seeded on poly-L-lysine coated coverslips in a 24-well plate, and cultured until confluent. The cells were transduced by addition of AAV9-NPC2-2A-GFP to their culture medium, in concentrations of $5x10^9$ or 10^{10} vg per well, followed by a gentle stirring of the plate. The cells were transduced for 48 h, after which the medium was changed. Following transduction, the cells were cultured for 10 days with a bi-weekly media change.

2.4.1 ICC on transduced astrocytes

ICC was performed on the AAV9-NPC2-2A-GFP transduced primary rat astrocytes to investigate the infectivity of AAV9-NPC2-2A-GFP, and to investigate whether they are able to express their transgene. The astrocytes were fixed as described in *section 2.2.8*, and stained with Rabbit anti-GFP to enhance detection of transduced cells with Alexa Fluor 488 secondary antibodies. Mouse-anti-GFAP was used as an astrocyte marker with Alexa Fluor 594 secondary antibodies. The ICC procedure was performed as described in *section 2.2.8.*

2.5 Effects of AAV9-NPC2-2A-GFP on an in vitro BBB model

To investigate the effects of AAV9-NPC2-2A-GFP in a setup more similar to in vivo conditions, an in vitro non-contact co-culture BBB model was set up, consisting of PBECs on filters submerged in wells with primary astrocytes, for transduction with AAV9-NPC2-2A-GFP.

2.5.1 Construction of in vitro BBB models

The primary rat astrocytes were cultured in poly-L-lysine coated (5 µg/mL) 12-well plates (cat. #665180, Greiner CELLSTAR®) with and without coverslips, under conditions described in *section 2.1.2.* They were kept in mono-culture for 2 weeks with a bi-weekly media change until confluent. Astrocyte conditioned media (ACM) was collected and sterile filtered from confluent astrocytes before co-culture with PBECs.

PBECs were seeded on filter inserts (ThinCerts™, cat. #665610, Greiner Bio-One) coated with collagen IV (0.5 mg/mL, cat. #C5533, Sigma-Aldrich) and fibronectin (0.1 mg/mL, cat. #F1141, Sigma-Aldrich) at a density of 155.000 cells/filter and cultured as described in *section 2.1.2* for 24 h before co-culture with primary rat astrocytes.

In order to induce BBB properties, filters with PBECs were washed in PBS and moved to wells with astrocytes and media was supplemented; PBECs received media (see *section 2.1.2*) supplemented with HC (550 nM, cat. #H4001, Sigma-Aldrich), cAMP (250 µM, cat. #C3912, Sigma-Aldrich) and RO (17.5 µM, cat. #B8279, Sigma-Aldrich), while astrocytes were kept in 50 % ACM and 50 % PBEC media, as specified in *section 2.1.2,* supplemented with HC (550 nM).

2.5.2 AAV9-NPC2-2A-GFP transduction of BBB models

For AAV9-NPC2-2A-GFP transduction of the barriers, 10^{10} vg were added per PBEC filter, followed by a gentle manual rocking of the plate. The cells were transduced for 48 h, after which media was changed to fresh medium,

described in *section 2.5.1*. The barriers were kept in culture for 10 days after addition of virus, with a media change every 3 days.

Because the Laboratory of Neurobiology, Aalborg University, DK has observed that PDS interferes with ELISA for quantitative detection of NPC2, media was replaced by media free of PDS (DMEM/F12 with 10 % FCS, 1 % ITS, gentamicin (10 µg/mL), bFGF (1 ng/mL) with supplementations specified in *2.2.3*) on the last media change before harvest, which was subsequently collected for analysis at the end of the experiment. Media substitution was held off until the last media change, because PDS keeps pericyte contamination at bay.

In order to monitor BBB integrity, TEER was measured daily throughout the experimental procedure, using a Millicell epithelial-volt-ohm meter and chopstick electrodes (Millipore). TEER was measured on 9 co-culture wells per condition, thus n-values are defined as n=9, even though co-cultures originated from the same batches of PBECs and primary astrocytes. Even though not representing biological replicates, it is worth noting that each isolation originated from several animals. Each well was measured in triplicates and normalized to a blank control. TEER was calculated as the mean of the well triplicates minus the mean of the control, and multiplied by the growth area of the filter inserts (1.12 cm^2). Data was collected in Excel 2016 and statistically analyzed in GraphPad Prism 6 by several Mann-Whitney non-parametric tests, comparing untreated filters to AAV9 treated filters for each day.

In order to ensure that untreated barriers served as an appropriate control for the setup, it was investigated whether addition of temperate or cold 1X PBS-MK (1X PBS with 1 mM $MgCl_2$ and 2.5 mM KCl), a substantial component of the virus solution vehicle, affected TEER compared to untreated co-cultures. One filter per condition was examined (n=1).

2.5.3 ICC for detection of transduction

ICC was performed on PBECs and primary rat astrocytes from the cultured BBB models to investigate the infectivity of AAV9-NPC2-2A-GFP and its expression of the transgene, as well as to visually investigate if addition of AAV9-NPC2-2A-GFP could have detrimental effects on the barriers.

Both cell types were stained with Rabbit anti-GFP (1:2,000 in blocking buffer) with Goat anti-rabbit Alexa Fluor 488-conjugated secondary antibodies (1:500 in blocking buffer) to enhance detection of transduced cells. Moreover, astrocytes were stained with a cell specific marker, Mouse-anti-GFAP. PBECs were stained with Mouse anti-ZO-1 (1:500 in blocking buffer, cat. #339100, Invitrogen) to give an indication of barrier integrity, as well as Mouse anti-α-SMA (1:500 in blocking buffer, cat. #A5228-2, Sigma), a pericyte marker. Goat anti-mouse Alexa Fluor 594-conjugated secondary antibodies (1:500 in blocking buffer) were added to the wells with anti-GFAP, ZO-1 and α-SMA. The ICC procedure was performed similar to the procedure described in *section 2.2.8.* Cells from untreated barriers were used as controls.

2.5.4 RT-qPCR on GFP and TJ proteins

To investigate whether transduction of PBECs with AAV9-NPC2-GFP induces a change in the expression of tight junction proteins ZO-1, ZO-2, Claudin-5, Claudin-12 and Occludin, their gene expression was investigated through RT-qPCR. Furthermore, qPCR using primers targeting GFP was investigated in PBECs and rat astrocytes as a sensitive method for detection of the transgene.

2.5.5 RNA purification and cDNA synthesis

RNA was purified using the GeneJET RNA Purification Kit (cat. #K0731, Thermo Scientific). After collection of the culture medium, cells were washed in PBS twice, and lysed with lysis buffer supplemented with β-mercaptoethanol (14.3 M, 1:50). Four wells or filters, respectively, were pooled, collected in Eppendorf tubes and vortexed for 10 s, prior to addition of ethanol (99 %, 0.6:1). Samples were then transferred to a GeneJet RNA Purification column placed in a collection tube, and centrifuged in a Universal 320 R centrifuge (Hettich) at 12,000 g for 1 min, and the flow-through was discarded. Next, columns were washed with Wash Buffer 1 and centrifuged for 1 min at 12,000 g, after which the flow-through was discarded. This was followed by two additional washes and centrifugations using Wash Buffer 2. Lastly, the RNA was eluted by transferring the purification columns to new RNase-free microcentrifuge tubes and adding nuclease-free water to the column, which was centrifuged at 12,000 g for 1 min, after which the eluate was collected. RNA concentrations were measured by spectrophotometry (DeNovix DS-11).

Following RNA purification, the RNA (100 ng/µL) was DNase treated to remove contaminating DNA by mixing it with reaction buffer with $MgCl_2$ (1X, cat. #B43, Thermo Scientific™) and RNase-free DNase I (0.1 U/µL, cat. #EN0521, Thermo Scientific™) in nuclease-free water, and incubating them at 37 °C for 30 min in a thermal cycler

(Applied Biosystems® Veriti® 96-Well). Subsequently, the DNase was inhibited by addition of 50 mM EDTA (1:11, Thermo Scientific™) and incubation at 65 °C for 10 min.

Lastly, RNA was reverse transcribed into cDNA using the RevertAid H Minus First Strand cDNA Synthesis Kit (cat. #K1631,Thermo Scientific™) by mixing RNA (90.91 ng/µL) with 25 pmol oligo $(dT)_{18}$ primer, 25 pmol random hexamer primers, 0.5 mM dNTP mix, 1X RT buffer and Maxima H Minus Enzyme Mix (1:20) in nuclease free water, and centrifuging briefly, prior to incubation at 25 °C for 10 min, 50 °C for 15 min, and 85 °C for 5 min in a thermal cycler. Controls testing for DNA contamination were prepared by subjecting DNase treated RNA samples to the cDNA synthesis procedure, leaving out Maxima H Minus Enzyme Mix.

2.5.6 qPCR

To analyze the expression of ZO-1, ZO-2, Claudin-5, Claudin-12 and Occludin in PBECs, the primers listed in *table 3* were used. Hypoxanthine phosphoribosyltransferase 1 (HPRT1) and β-actin served as housekeeping genes. To analyze transcriptional activity of the transgene, primers against GFP were analysed on both primary rat astrocytes and PBECs, and normalized to HPRT1 and β-actin specific to their species. Test of GFP-primer efficiency is described in *appendix 5*. Optimal primer efficiencies for the remaining primers were previously confirmed by the laboratory by standard curves.

For the reaction, 2.5 ng cDNA in Tris-HCl was loaded in a 96-well PCR plate (cat. #AB-0900, Thermo Scientific™) in triplicates, followed by Maxima SYBR Green with ROX passive reference dye and a forward primer (10 pmol), and reverse primer (10 pmol) for each of the genes. The plate was spun down before the reaction was run on a Stratagene Mx3005P qPCR system (Agilent Technologies) coupled to the Stratagene MxPro qPCR data analysis software (v4.10). The qPCR run was initialized by a denaturation step at 95 °C for 10 min to activate the Maxima Hot Start Taq DNA Polymerase, followed by 40 cycles of denaturation phases at 95 °C for 30 s, annealing phases at 60 °C for 30 s, and elongation phases at 72 °C for 30 s, and a subsequent melting curve at 95 °C for 1 min, 30 s at 55 °C, and 30 s at 95 °C.

The relative expression (RE) was calculated using the following formula with inspiration from the Pfaffl method [114]: $RE = (1 + \text{primer efficiency})^{-Ct}$, in which primer efficiency was set to 1, and Ct denotes the mean cycle threshold from each triplicate.

The normalized fold change of target genes was then calculated by dividing their RE with the geometric mean of the RE of the housekeeping genes:

$$Normalized\ fold\ change = \frac{RE\ of\ target\ gene}{Geometric\ mean\ of\ HRT1\ and\ \beta - actin}$$

Gene	**Primer sequences**	**Target**
Porcine β-Actin	Forward: 5'-CAGAGCGCAAGTACTCCGTGTGGAT-3' Reverse: 5'-GCAACTAACAGTCCGCCTAGAAGCA-3' Product size: 147 bp	XM_003124280.5 Sus scrofa actin beta (ACTB), transcript variant X1, mRNA
Porcine HPRT1	Forward: 5'-AATGCAAACCTTGCTTTCCTTGGTC-3' Reverse: 5'-GGCATAGCCTACCACAAACTTGTCT-3' Product size: 151 bp	NM_001032376.2 Sus scrofa hypoxanthine phosphoribosyltransferase 1 (HPRT1), mRNA
Porcine ZO-1	Forward: 5'-AAGCCTCCAGAGGGAGCATCTAA-3- Reverse: 5'-ATATCTTCAGGTGGCTTCACTTGGG-3' Product size: 146 bp	XM_021098827.1 Sus scrofa, tight junction protein 1 (TJP1), transcript variant X1 to X15, mRNA
Porcine ZO-2	Forward: 5'-ACAGAGGTTGAACCCATCATCCAAC-3' Reverse: 5'-AATTGTGTCCTTCAAGCTGCCAAAC-3' Product size: 151 bp	NM_001206404.1 Sus scrofa tight junction protein 2 (TJP2), mRNA
Porcine Claudin-5	Forward: 5'-GTCTTGTCTCCAGCCATGGGTTC-3' Reverse: 5'-GTCACGATGTTGTGGTCCAGGAAG-3' Product size: 140 bp	NM_001161636.1 Sus scrofa claudin 5 (CLDN5), mRNA

Porcine Claudin-12	Forward: 5'-GTTTCACACACGACCTAACAGGGAA-3' Reverse: 5'-TGGCTTCATTGACTGGTCAGAAACA-3' Product size: 133 bp	XM_005667576.3 Sus scrofa claudin 12 (CLDN12), transcript variant X1, mRNA
Porcine Occludin	Forward: 5'-GCCCATCCTGAAGATCAGGTGAC-3' Reverse: 5'-CTCCACCATATATGTCGTTGCTGGG-3' Product size: 132 bp	NM_001163647.2 Sus scrofa occludin (OCLN), mRNA
Rat β-Actin	Forward: 5'-CCTCTGAACCCTAAGGCCAACCGTGAA-3' Reverse: 5'-AGTGGTACGACCAGAGGCATACAGGG-3' Product size: 123 bp	NM_031144.3 Rattus norvegicus actin, beta (Actb), mRNA
Rat HPRT1	Forward: 5'-TGCAGACTTTGCTTTCCTTGGTCA-3' Reverse: 5'-TGGCCTGTATCCAACACTTCGAG-3' Product size: 103 bp	NM_012583.2 Rattus norvegicus hypoxanthine phosphoribosyltransferase 1 (Hprt1), mRNA
GFP	Forward: 5'-CTGGACGGCGACGTAAACGG-3' Reverse: 5'-CAGGGTCAGCTTGCCGTAGG-3' Product size: 81 bp	Transgene: Enhanced GFP. Present in CMV-EPO-GFP and pFastbac-AAV-CAG-NPC2-2A-GFP

Table 3: *Overview of primers for RT-qPCR on primary porcine brain endothelial cells and primary astrocytes. Primers were ordered from TAG Copenhagen.*

2.5.7 Detection of secreted NPC2 via ELISA

An ELISA was performed on the pooled medium harvested from the in vitro barriers (9 co-culture wells or filters per condition), described in *section 2.5.2,* to evaluate if transduction with AAV9-NPC2-2A-GFP could have a potential therapeutic effect by upregulating the NPC2 production in the cell types of the barrier. The ELISA was performed using a Human NPC2 ELISA kit (cat. #SEK13341, Sino Biological), according to manufacturer's instructions. Buffer and stock contents are listed in *table 4*.

A Nunc MaxiSorp™ flat bottom transparent 96- well plate (cat. #44-2404-21, Invitrogen™) was prepared by coating the wells with rabbit anti-Human NPC2 monoclonal capture antibody (2 µg/mL in sterile-filtered K-PBS, cat#13341-R034, Sino Biological), after which the plate was sealed and incubated overnight at 4 °C. Next, the wells were washed three times with Wash buffer. The wells were then blocked by addition of Blocking buffer, and the plate was incubated for 1 h at RT. The wells were washed three additional times, after which the samples were loaded, and the plate was sealed and incubated for 2 h. Next, the wells were washed three times, followed by addition of rabbit, anti-Human NPC2 monoclonal detection antibody conjugated to horseradish-peroxidase (0.15 µg/mL in sterile filtered Detection antibody dilution buffer, cat. #13341-R031, Sino Biological), and the plate was sealed and incubated for 1 h. The washing step was repeated, and freshly made Substrate Solution was added, containing Substrate stock (10 mg/mL Tetramethylbenzidine in DMSO, cat. #860336, Sigma Aldrich) and Substrate dilution buffer in a ratio of 1:100, supplemented with 0.0024% H_2O_2 (cat. #88597, Sigma Aldrich). The plate was then incubated for 20 min protected from light. Finally, stop solution containing 2N H_2SO_4, was added to the wells, and optical density was measured immediately on a PerkinElmer EnSpire® Multimode Plate Reader set to 450 nm. All incubation steps were performed while on a Belly Dancer® shaker, and all samples were run in duplicates. A standard was made on 2-fold 7-point dilutions of recombinant Human NPC2 in sterile filtered Sample dilution buffer, with a high standard of 10,000 pg/mL. Data analysis was performed in Excel 2016, according to manufacturer's protocol, and data was illustrated in GraphPad Prism 6.

Stocks and buffers	**Content**
Tris- buffered saline (TBS)	20 mM Tris, 150 mM NaCl
Wash buffer	0.05% Tween® 20 (cat. #P1379, Sigma Aldrich) in TBS
Blocking buffer	2% BSA in Wash Buffer

Detection antibody dilution buffer	Wash Buffer with 0.5% BSA
Substrate dilution buffer	0.05 M Na_2HPO^4 and 0.025M citric acid
Sample dilution buffer	0.1% BSA in Wash buffer

***Table 4**: Content of buffers used in the ELISA.*

2.6 Optimization of promoters

To optimize the process of detecting positively transfected or transduced cells, a promoter study was set up to investigate how a difference in promoter could affect the measured transfection efficiency. This optimization study focuses on the CAG promoter, which is upstream of the gene of interest in the AAV9-NPC2-2A-GFP investigated in this study, and compares it to the CMV promoter.

2.6.1 Cloning

To evaluate differences between CAG and CMV, a setup was first made to produce plasmids with the same gene of interest and same fluorescent tags with each of the promoters.
Primers were designed to amplify NPC2-2A-GFP from the pFastbac-CAG-NPC2-2A-GFP plasmid (*table 5*) through PCR, to subsequently insert it into the the backbone of pCMV-NPC2-OFPSpark (cat. #MG52313-ACR, Nordic Biosite™), replacing NPC2-OFPSpark, and creating a pCMV-NPC2-2A-GFP plasmid (see *figure 4*). The newly cloned plasmid can thus be experimentally compared to pFastBac-CAG-NPC2-2A-GFP with greater accuracy due to the identical transgenes.

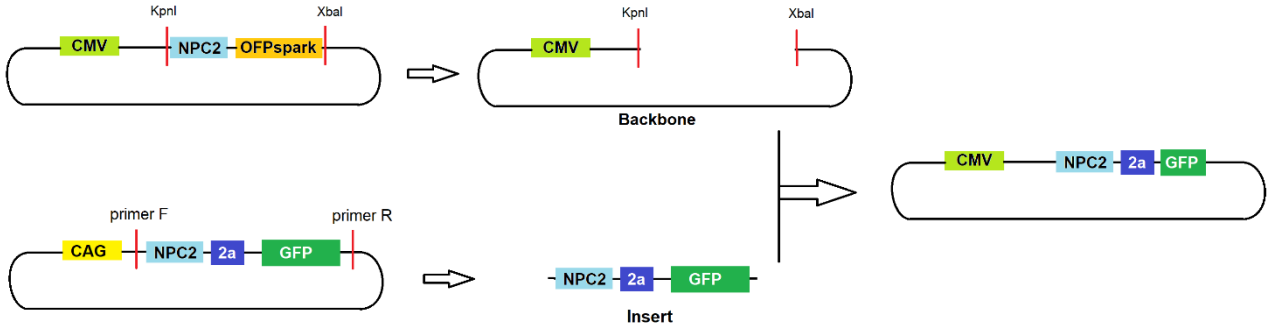

***Figure 4**: Illustration of cloning strategy.*

2.6.1.1 Preparation of insert

Forward- and reverse primers were designed to amplify the NPC2-2A-GFP insert (*table 5*). 6 nonsense bases followed by a restriction site for KpnI was added on to the 5' end of the forward primer, while 6 nonsense bases followed by a restriction site for XbaI was added on to the 5' end of the reverse primer, thus allowing for subsequent restriction digest and sticky end ligation.

Amplification of the insert was performed using the Phusion High Fidelity DNA Polymerase kit (cat. #F530S, Thermo Scientific™). For the PCR reaction, 10 ng of template DNA (pFastbac-CAG-NPC2-2A-GFP) was mixed with Phusion HF-buffer (1X), dNTPs (200 µM each), forward primer (0.5 µM), reverse primer (0.5 µM), DMSO (3 %), and Phusion Polymerase (0.02 U/µL) in nuclease free water.

The PCR reaction was run in a Veriti™ 96-Well Thermal Cycler (Applied Biosystems) with an initial denaturation step at 98°C for 30 s, followed by a 2-step protocol with 30 cycles of denaturation at 98°C for 7 s and annealing/extension at 72°C for 2 min, and a final extension at 72°C for 7 min.

Afterwards, the size of the PCR product was validated by gel electrophoresis. The sample was mixed with loading dye (1X, cat. #R0611, Thermo Scientific™) and loaded in an agarose gel (1 % agarose in Tris-acetate-EDTA with 1X GelRed™) along with a 1 kb ladder (cat. #SM0313, Thermo Scientific™) and run at 100V. The bands were visualized through an Odyssey Fc Infrared Imaging System (Li-Cor).

Before digestion, the Machery-Nagel NucleoSpin® Gel and PCR Clean-up kit was used to purify the PCR product in order to remove the active thermophilic DNA polymerase, thus reducing the likelihood that it alters the ends of the cleaved DNA.

The PCR product was mixed with NTI-buffer (1:2) and centrifuged in a NucleoSpin® clean-up column at 11,000 g for 30 s to bind DNA, and the flow-through was discarded. Next, NT3-buffer was loaded and centrifuged at 11,000 g for 30 s to wash the silica membrane. The flow-through was discarded, and the washing step was repeated. This was followed by centrifugation at 11,000 g for 2 min to dry the silica membrane. Because ethanol from the NT3-buffer may inhibit subsequent enzymatic reactions, the residual ethanol was evaporated by incubation of the sample at 50 °C in a heating block, lid open. Lastly, the DNA was eluted by addition of NE-Buffer, which was left to incubate for 5 min at RT, before it was collected in a collecting tube by centrifugation at 11,000 g for 1 min. The elution step was repeated with the same eluate to increase yield. DNA concentrations were measured by spectrophotometry, before the insert was digested by restriction enzymes, producing sticky ends. DNA (50 µg/µL) was mixed with FD Green Buffer (1X), FD KpnI (1X) and FD XbaI (1X, cat. #FD0684, Thermo Scientific™) in nuclease free water. The reaction was gently mixed and spun down, after which it was incubated at 37 °C for 10 min.

The digested insert was then subjected to gel purification using the Machery-Nagel NucleoSpin® Gel and PCR Clean-up kit. First, the digested insert was run in a low melting temperature gel (1 % BacPlaque™ Agarose, cat. #70034-30GM, Novagen® and 1X GelRed™ in Tris-acetate-EDTA) at 100V and the band was excised with a scalpel on a UV Table (Vilber Lourmat). The sliced gel was then mixed with NTI-buffer (2 µL NTI-buffer pr. mg gel) in an eppendorf tube. The sample was incubated at 50 °C with brief vortexing every 2-3 min until all gel had dissolved. It was then transferred to a NucleoSpin® clean-up column, in which it was centrifuged at 11,000 g for 30 s, and the flow-through discarded. This was followed by two washes with NT3-buffer, which was centrifuged at 11,000 g for 30 s and the flow-through discarded. Following washes, the silica membrane was dried by centrifugation at 11,000 g for 2 min, and residual ethanol was evaporated by incubation in a heating block at 50 °C, lid open. The DNA was eluded by addition of Buffer NE, which was left to incubate for 5 min at RT, and collected in a collecting tube by centrifugation at 11,000 g for 1 min. The elution step was repeated with the same eluate to increase yield.

Cloning_insert_F_NPC2-2A-GFP	5’-GATGGTGGTACCATGCGTTTTCTGGCCGCCACGA-3’
Cloning_insert_R_NPC2-2A-GFP	5'-CGATAGTCTAGAAGGCTGATCAGCGAGCTCTAGTC-3'
Colony_F_pCMV-NPC2-2A-GFP	5'-ATGGGCGGTAGGCGTGTACG-3'
Colony_R1_pCMV-NPC2-2A-GFP	5'-GGACTGGTAGCTCAGGTAGTGGTT-3'
Colony_R2_pCMV-NPC2-2A-GFP	5'-GGCAAACAACAGATGGCTGGCAA-3'

***Table 5**: Primer sequences for NPC2-2A-GFP amplification, and pCMV-NPC2-2A-GFP screening. Primers were ordered from TAG Copenhagen.*

2.6.1.2 Preparation of backbone

The pCMV-backbone was prepared by restriction digest of pCMV-NPC2-OFPSpark, in which the old insert was removed. DNA (50 ng/µL) was mixed with FD Green Buffer (1X), FD KpnI (1X) and FD XbaI (1X) in nuclease free water. The reaction was gently mixed and spun down, after which it was incubated at 37 °C for 10 min.

The product of the restriction digest was analyzed through gel electrophoresis, following the same procedure as for the insert (see *section 2.6.1.1*), to validate that the band size corresponding to the backbone was present, and to ensure that the old insert had been cut out.

Next, the digested DNA was run at 100V in a low melting temperature 1 % agarose gel, and the band corresponding to the pCMV-backbone was cut under UV, and purified using the Macherey-Nagel NucleoSpin® Gel and PCR Clean-up kit following the same protocol as specified in *section 2.6.1.1.* The band corresponding to the old insert (NPC2-OFPSpark) was cut and purified separately for use as a positive control for ligation.

2.6.1.3 Ligation and transformation

pCMV (0.020 pmol) and NPC2-2A-GFP (0.060 pmol) were ligated in a reaction with T7 DNA Ligase Reaction Buffer (1X, cat. #M0318L, NEB), ATP (0.5 mM, cat #R0441, Thermo Scientific™), DL-Dithiothreitol (0.5 mM, cat.

#D-0632, Sigma-Aldrich) and T7 DNA Ligase (150 U/µL, cat. #M0318L, NEB) in nuclease free water, which was incubated for 30 min at RT. pCMV (0.020 pmol) and NPC2-OFPSpark (0.060 pmol) were subjected to the same procedure as a positive control for the ligation reaction.

The ligated plasmids were amplified by transformation of chemically competent E. coli. The ligation mix was added to chemically competent E. coli in a 1:5 ratio, and the tube was flicked to mix, followed by incubation on ice for 30 min. The tube was then placed in a water bath at 42 °C for 20 s to heat shock the cells, and put back on ice for 2 min. Subsequently, SOC medium was added, followed by 1 h incubation at 37°C and 200 RPM. Lastly, the mixture was spread on agar plates with kanamycin monosulfate (50 µg/mL, cat. #25389-94-0, Sigma-Aldrich™).

A positive control for transformation was prepared with undigested pCM3-NPC2-OFPSpark, and a negative control was prepared with a plasmid with ampicillin resistance (pFastbac-CAG-Luciferase).

2.6.1.4 Screening colonies (colony PCR)

Small, sharply outlined bacterial colonies were picked with a pipette and first transferred to an agar plate (50 µg/mL kanamycin), then resuspended in nuclease-free water and subsequently in LB media with 50 µg/mL kanamycin. The bacteria in the LB solution were left to incubate overnight at 37°C and 200 RPM, while the bacteria in nuclease-free water were lysed by heating them to 99°C for 7 min, and used as template for colony PCR. Two separate reactions were run for each clone with different reverse primers (listed in *table 5*). The forward primer starts in the CMV-promoter within the backbone, and reverse primer 1 was designed to start in the GFP-tag within the insert, thus ensuring ligation of backbone and the correct insert. Reverse primer 2 was designed to start in the backbone after the insertion site, hereby testing successful ligation in both ends of the insertion site. The positive result of the reverse primer 1 amplicon also ensures that the backbone has not self-ligated without incorporation of the insert (see *figure 5* for illustration).

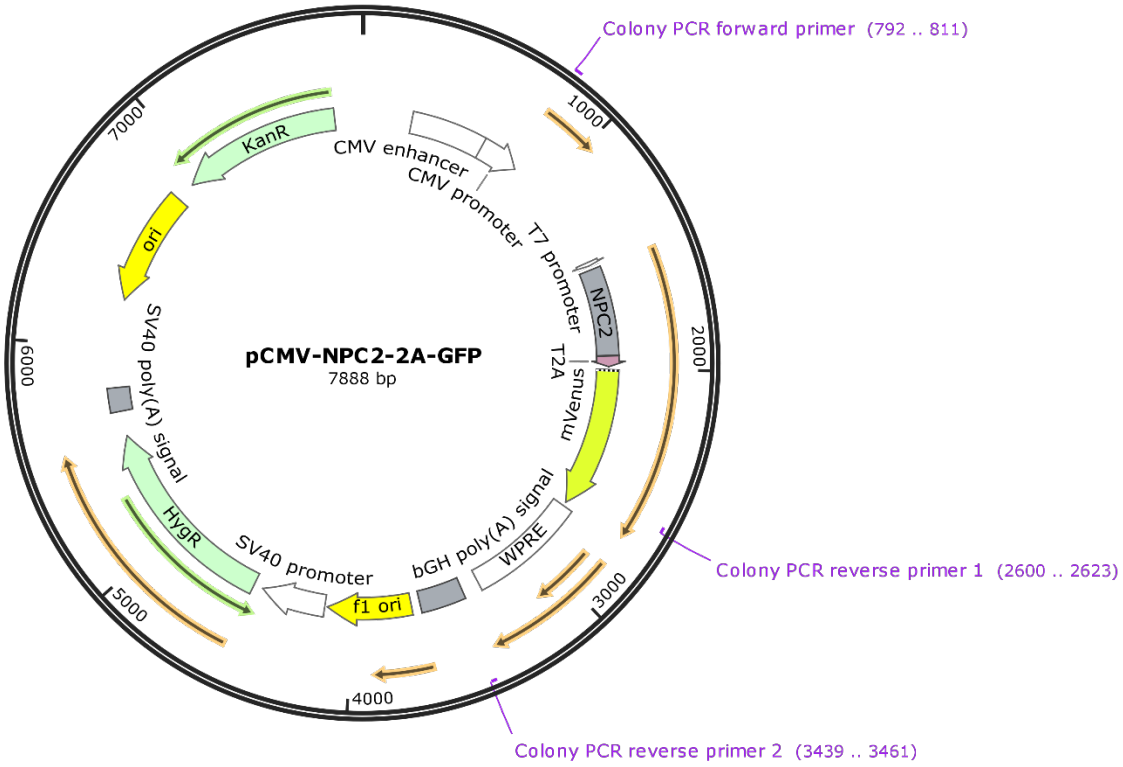

Figure 5: *Illustration of forward and reverse primers used to screen colonies for the cloned plasmid. Plasmid map made using SnapGene® Viewer.*

For the PCR reaction, bacterial colony lysates were mixed with DreamTaq Green PCR Master Mix (1X, cat. #K1081, Thermo Scientific™), 0.4 µM forward primer and 0.4 µM reverse primer 1 or 0.4 µM reverse primer 2 in nuclease-free water. The PCR reaction was run in a Veriti™ 96-Well Thermal Cycler with an initial denaturation step at 95°C for 5 min, followed by a 3-step protocol with 30 cycles of denaturation at 95°C for 30 s, annealing at 60 °C for 30 s, extension at 72°C for 2 min 30 s, and a final extension phase at 72°C for 5 min.

Products were analyzed through gel electrophoresis in a 1 % agarose gel following the same procedure as specified in *section 2.6.1.1*, to ensure the final product correlates with the expected DNA sequence lengths.

2.6.1.5 Investigation of the cloned plasmid

The final cloned product did not correlate with expectations (see *appendix 6*), hence the plasmid was further analyzed by restriction analysis, transfection of HeLa cells and visualization of transgene by fluorescence microscopy. The cloned plasmid was amplified and purified as described in *sections 2.2.1* and *2.2.3*, but substituting ampicillin in the agar plates and LB medium for 50 µg/mL kanamycin. The restriction digest was performed with XhoI as described in *section 2.2.4* (see *appendix 6*).

Hela cells were transfected with the purified cloned plasmid for visualization of GFP transgene by fluorescence microscopy. 24 h before transfection, HeLa cells were seeded on coverslips in a 24 well-plates at a density of 18.000 cells/cm2. For transfection, 1 µg of DNA (either the purified cloned plasmid or pFastbac-CAG-NPC2-2A-GFP as a positive control) was mixed with 100 µL serum-free growth medium and 2 µL TurboFect™ Transfection Reagent (cat. #R0532, Thermo Scientific™) per well, which was vortexed thoroughly and incubated for 15 min at RT. The transfection solution was added dropwise to the culture medium and plates were gently swirled. Untransfected controls received 100 µL plain serum-free medium. After transfection, cells were kept in a standard incubator for 48 h until fixation. The cells were fixated, blocked, DAPI stained, mounted and examined as described in *section 2.2.8*, however no immunostaining was needed (see *appendix 6* for results).

2.6.2 Testing promotor effects on quantification of transfection

Cloning of the CMV-NPC2-2A-GFP plasmid did not succeed. Instead the CMV-EPO-GFP plasmid (cat. #RG80055-ACG, Sino Biological™), was used as an alternative. Hence pFastbac-AAV-CAG-NPC2-2A-GFP was compared to CMV-EPO-GFP, to investigate whether promoters influence transcription efficiency of the gene of interest and thus indirectly the measurable transfection efficiency. To investigate differences between the CAG and CMV promoters, expression was measured at the protein level via flow cytometry and ICC. Because the two plasmids contain the same fluorescent tag, it makes comparisons more valid.

2.6.2.1 Transfection of HeLa- and bEnd.3 cells

24 h prior to transfection, HeLa cells and bEnd.3 cells passage #6 to #14 were seeded in 24 well-plates at a density of 18,000 cells/cm^2. Cells for ICC were seeded on coverslips. Transfection with pFastbac-AAV-CAG-NPC2-2A-GFP or pCMV-EPO-GFP was performed as described in *section 2.6.1.5*. Untransfected cells were used as controls. After transfection, cells were kept in a standard incubator for 48 h until fixation, harvesting of RNA or trypsinization for flow cytometry.

2.6.2.2 ICC on HeLa and bEnd.3 cells

Transfected cells were investigated by fluorescence microscopy to visualize expression of the transgene via the self-fluorescent tag GFP, allowing direct comparison, and via immunostaining of NPC2 or EPO, allowing differentiation between the two plasmids. 48 h after transfection, cells were fixated as described in *section 2.2.8*, and stored in PBS at 4°C protected from light for no more than three days before ICC was performed. The ICC procedure was performed as described in *section 2.2.8*.

Cells transfected with pFastbac-AAV-CAG-NPC2-2A-GFP were stained with Rabbit anti-NPC2 antibodies (1:500 in blocking buffer, cat. #HPA000835, Sigma-Aldrich), and Goat anti-rabbit Alexa Fluor 594-conjugated secondary antibodies (1:500 in blocking buffer). Cells transfected with pCMV-EPO-GFP were stained with Rabbit anti-EPO antibodies (1:500 in blocking buffer, cat. #SC-7956, Santa Cruz Biotechnology), and Goat anti-rabbit Alexa Fluor 594-conjugated secondary antibodies (1:500 in blocking buffer). Untreated cells were stained with each of the antibody conditions, respectively, and used as negative controls. Fluorescence microscopy and image processing were performed as described in *section 2.2.8*.

2.6.2.3 Flow cytometry on HeLa- and bEnd.3 cells

Flow cytometry was performed on the transfected cells to quantify measurable positively transfected cells by their transgene protein expression. As untransfected cells had previously been verified to serve as a suitanle negative control when measuring transfection efficiency in flow cytometry (see *appendix 8*), untransfected cells were used as a negative control. 48 h after transfection, cells were prepared for flow cytometry and analyzed on the CytoFLEX Flow Cytometer

as described in *section 2.3.2* with modified acquisition settings, as the FITC channel was set to 45. The experiment was conducted in HeLa cells once, pooling 6 wells into 2 samples, thus the n-value was defined n=2. The experiment was performed in bEnd.3 cells twice with different passages at different time points. In total, 18 wells were pooled into 6 samples, thus the n-value was defined n=6, and data was statistically analyzed by a non-parametric Mann-Whitney test. All data was analyzed and visualized in GraphPad Prism 6.

2.7 Establishing a Luciferase-assay for enhanced detection

Because luciferase is a highly sensitive reporter[115], a protocol for detection of transfection efficiency with plasmid DNA encoding firefly luciferase was established. The intention was to apply the established assay to detect AAV9 transduction in vitro with greater sensitivity, as the insert cassette in AAV9 production may be exchanged for one with a luciferase reporter.

HBMEC passage #5, bEnd.3 passage #11, RBE4 passage #13, and HeLa cells were seeded in a white, opaque 96-well plate (cat. #655083, Greiner CELLSTAR®) at a density of 10^4 cells pr. cm^2 24 h before transfection, and maintained as specified in *section 2.1.1.* Wells assigned for RBE4 cells were coated with a collagen solution (0.1 mg/mL bovine collagen type I in 0.01 M HCl, cat. #354231, Corning™) prior to seeding of cells.

Prior to transfection, plasmid DNA encoding luciferase (pFastbac-CAG-Luciferase), provided by Eva Hede Olsen (Laboratory of Neurobiology, Aalborg University), was amplified and purified as specified in *sections 2.2.2* and *2.2.3*, and subjected to restriction analysis using the same procedure as elaborated upon in *section 2.2.4* using the enzymes SmaI, a double digest with XhoI and NdeI, and Cfr42I (cat. #ER0201, Thermo Scientific™) and compared to the plasmid stock (see *appendix 4*). Only SmaI digest revealed the expected bands, referencing the sequence (*appendix 4*), but since the amplified plasmid revealed bands corresponding to the stock, pFastbac-CAG-Luciferase was used in the assay.

For transfection, 0.2 µg DNA was mixed with 40 µL serum-free growth medium and 0.4 µL TurboFect™ Transfection Reagent per well, vortexed thoroughly and left to incubate at RT for 15-20 min. Hereafter, the transfection solution was added dropwise to the growth medium in each well, and the plate was rocked to allow even distribution of DNA-complexes. Non-transfected controls received 40 µL serum free media. 8 wells of each cell type were transfected, and 8 were left non-transfected for negative controls, of which one well per condition was used as a non-luciferin control. Thus, the n-value was defined as n=7, although it does not represent biological replicates.

After 24 h, media was changed to media with XenoLight D-Luciferin Bioluminescent Substrate (150 µg/mL, cat. #122799, PerkinElmer®). Non-luciferin controls received plain media. Immediately after media change, luminescence was measured every 5 min for a total of 10 repeats on a PerkinElmer EnSpire® Multimode Plate Reader at 37 °C.

After measuring luminescence, a bicinchoninic acid assay was performed on the cells using the Thermo Scientific Pierce™ BCA protein assay kit, in order to normalize relative light units (RLU) to protein concentrations. First, media was removed, and the wells washed in PBS. The samples were then lysed with lysis buffer (150 mM NaCl, 2 mM $MgCl_2$, 2 mM $CaCl_2$, 10 mM HEPES, Triton X-100 (1:100, cat. #X100-100ML, Sigma-Aldrich)) with a cOmplete™ Mini EDTA-free protease inhibitor cocktail (1 tablet pr. 10 mL lysis buffer, cat. #11836170001, Roche). An albumin standard curve was then prepared according to manufacturer's instructions, and samples and standards were loaded in a 96-well plate (cat. #665180, Greiner CELLSTAR®), followed by 200 µL Working Reagent. The plate was mixed on a plate shaker for 30 s, followed by 1 h incubation at 37 °C while protected from light. Following incubation, the absorbance at 562 nm was measured on a PerkinElmer EnSpire® Multimode Plate Reader.

Blank corrected protein concentrations in each sample were calculated from the BCA standard curve by the Multimode Plate Reader software and exported to Excel (Microsoft Office 2016). In addition, kinetic measurements of luminescence was exported to Excel as RLU, blank corrected, and subsequently normalized to their corresponding protein concentrations. Data was analyzed in Graphpad Prism 6 as RLU/µg protein. Differences between transfected and non-transfected cells at 20 min post luciferin addition were compared by multiple Mann-Whitney non-parametric tests.

3. Results and discussion

3.1 Investigation of the produced AAV9-NPC2-2A-GFP

AAV9-NPC2-2A-GFP vectors were produced with the purpose of transducing in vitro BBB models. AAV9-NPC2-2A-GFP-P, containing vg from the cell pellet, as well as AAV9-NPC2-2A-GFP-S1 and AAV9-NPC2-2A-GFP-S2,

containing vg from the supernatant with one or two final centrifugations, respectively, were analyzed for titer and infectivity in the following sections.

3.1.1. Quantity of produced AAV9-NPC2-2A-GFP

The titers of AAV9-NPC2-2A-GFP-P, AAV9-NPC2-2A-GFP-S1 and AAV9-NPC2-2A-GFP-S2 were evaluated through absolute qPCR. The distribution of the vg between the three samples are illustrated in *figure 6.*

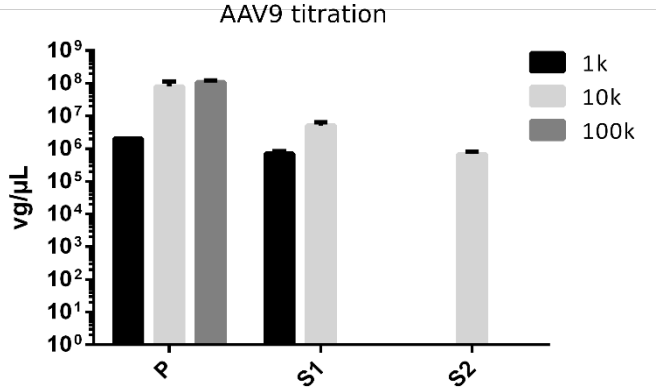

Figure 6: *Titer of AAV9-NPC2-2A-GFP-P, AAV9-NPC2-2A-GFP-S1 and AAV9-NPC2-2A-GFP-S2 determined through absolute qPCR, in samples diluted 1000, 10,000 and 100,000 times, respectively, which was accommodated for in the statistical analysis. Data is presented as mean ±standard deviation of technical duplicates. Some dilutions of the samples were excluded due to unspecific amplification assessed by the melting curves, as described in appendix 1.*

Based on the titration results, the absolute concentration of AAV9-NPC2-2A-GFP-P and AAV9-NPC2-2A-GFP-S1, respectively, are difficult to determine, as the results stretch from $2.05x10^6$ vg/µL to $1.18x10^8$ vg/µL in the AAV9-NPC2-2A-GFP-P sample, and $6.20x10^5$ vg/µL to $6.04x10^6$ vg/µL in the AAV9-NPC2-2A-GFP-S1 sample, depending on the dilution. Based on the melting curves, however, the 10.000 dilution titers were deemed most reliable (for elaboration, *see appendix 1*), which yielded concentrations of $5.16x10^7$ vg/µL for AAV9-NPC2-2A-GFP-P, $5.15x10^6$ vg/µL for AAV9-NPC2-GFP-S1 and $6.73x10^5$ vg/µL for AAV9-NPC2-2A-GFP-S2 (see *figure 6)*.

As the dilutions were accommodated for in the statistical analysis of the data, the results from the different dilutions should in theory amount to the same number of vg. However, it could appear that the more diluted the sample was, the higher the amount of vg/µL. The samples had not undergone iodixanol ultracentrifugation as the last centrifugation step, which is an important step in standard protocols of AAV purification [116,117]. The purification by ultracentrifugation in an iodixanol gradient enhances separation of virus from empty capsids, proteins, DNA and other components of cell debris. Thus, it is possible that the samples contained components which interfered with- and inhibited the polymerase reaction. Dilution of the samples would thereby also result in dilution of the potential inhibiting factor. This highlights the importance of iodixanol centrifugation in the purification process of AAV9 [118,119]. Indeed, if the polymerase reaction was inhibited by an unknown component within the solution, absolute qPCR may have been ill-suited for titration of this recombinant vector.

The absolute qPCR titration method performed in the current study is based on denaturation of capsid proteins, exposing the transgene, after which the CAG-promoter is amplified. The advantage to this method is that it can be used to titrate AAVs with different capsids and with different transgene cassettes, as long as they utilize the CAG promoter, hence it is practically applicable for a variety of virus stocks. In theory, this method should only measure DNA in intact virions as unpacked DNA would have been degraded in a preluding Benzonase digest. When samples are not purified by the iodixanol ultracentrifugation step, the Benzonase digestion step is particularly important, and even slight suboptimal conditions at this procedure could result in amplification of unpackaged DNA and a false high titer.

Another disadvantage to the absolute qPCR titration method is the many intermediate processing steps involved in dissolving the stock followed by amplification, in which even minor manual imprecisions could impact the outcome. Furthermore, this method relies on a standard curve, which consists of known concentrations of a plasmid containing the CAG-promoter. A disadvantage to this standard is that the plasmid DNA degrades over time; we have observed that even one freeze-thaw cycle impacts the concentration of the DNA, which was used to make the standards. This may impact the measured titers, making them appear higher than the true titer of the samples.

To accommodate these potential issues, other titration methods could be utilized in further studies. An alternative titration method could be an ELISA. Although concentrations of standards in this assay may also be reduced over freeze-thaw cycles, this assay has other advantages over the absolute qPCR, as it measures capsid proteins of the virus, which could reduce the risk of inadvertently measuring quantities of unpackaged plasmid DNA.

Additionally, intact virus titers could be quantified by functional assays, measuring infectious units, e.g. median tissue culture infective dose ($TCID_{50}$) or infectious center assay [120]; these assays are based on the ability of recombinant vectors to replicate within the nucleus of HeLa-derived cells expressing AAV2 *rep* and *cap* genes, when they are subsequently infected with a helper virus. Afterwards, the vector genome replication is determined, either via qPCR in the case of $TCID_{50}$, or via whole cell DNA hybridization using a labelled probe, targeting a part of the rAAV genome. These data may be normalized e.g. to ELISA-results, after which a ratio between total virions (ELISA) and infectious units can be obtained [120]. This is useful because the formation of a virion with capsid proteins is unfortunately no guarantee for infectious capability, as the capsid composition may be ineffective. This information on infectivity is an advantage, especially for clinical applications, for which quality control is particularly important. It may also be worth the effort and cost to evaluate the titers through functional assays prior to animal studies, both for ethical reasons and to prevent unnecessary monetary losses. Another, more simple approach, may be to transduce a permissive cell line, e.g. HeLa cells and analyze transgene expression via flow cytometry, similar to our investigations of transduction efficiency in *section 3.2*, which can provide a titer described as transducing units [120].

The suggested assays might be more expensive titration methods, but comparatively, it may be worth the initial cost in the long term, as the results would likely be more representative of actual titer, and additionally indicate that capsid formation has taken place, and that functionality is intact.

3.1.2 Infectivity and toxicity of produced AAV9-NPC2-2A-GFP

The infectivity and toxicity of the produced AAV9-NPC2-2A-GFP were evaluated by transduction of primary astrocytes, followed by immunostaining. By visual inspection of the viral solutions, AAV9-NPC2-2A-GFP-S2 appeared less cloudy than AAV9-NPC2-2A-GFP-S1, and as the concentrations were within a comparable range, a choice was made to only continue the investigation of AAV9-NPC2-2A-GFP-S2. In addition, AAV9-NPC2-2A-GFP-P was used for infection, despite a very cloudy appearance, because it had the highest titer. Results are illustrated in *figure 7*. Primary- and secondary antibody controls are illustrated in *appendix 2*.

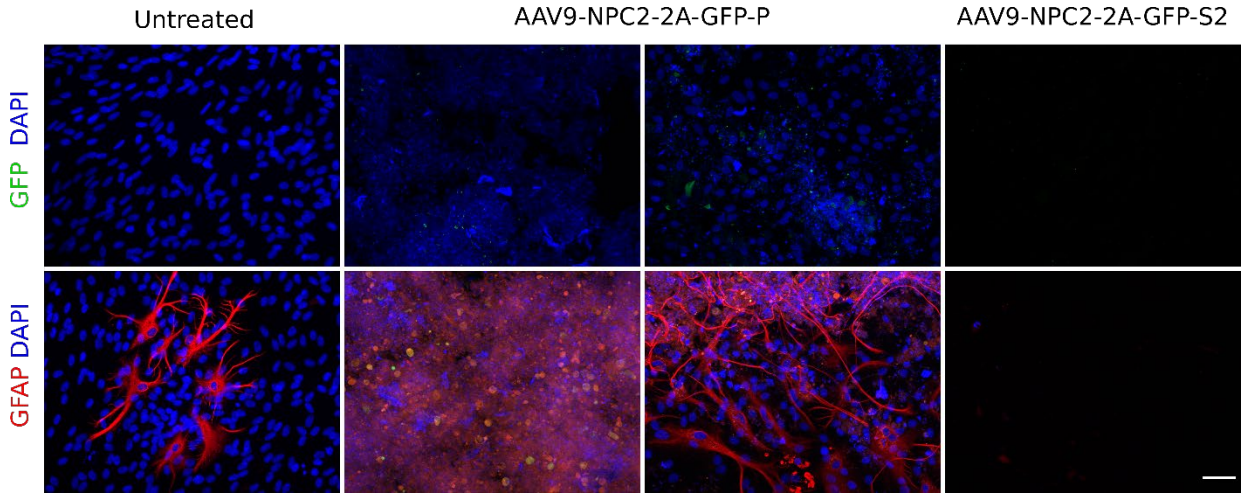

Figure 7: *Representative immunofluorescent images of primary rat astrocytes transduced with AAV9-NPC2-2A-GFP-P ($8.3x10^9$ viral genomes (vg) pr. well) and AAV9-NPC2-2A-GFP-S2 ($1.1x10^9$ vg pr. well), respectively, and untreated controls. GFAP-expression is depicted in red, and nuclei are stained with DAPI (blue). The GFP tag was immunostained for a stronger signal, and expected to show in green, but it was not detectable, indicating that no cells were transduced. Astrocytes in AAV9-NPC2-2A-GFP-P-treated wells had detached in areas covered by a veil of cell debris. An overall detachment of astrocytes was observed in AAV9-NPC2-2A-GFP-S2-treated wells. Scale bar = 50 µm.*

The immunostainings of AAV9-NPC2-2A-GFP-P treated astrocytes appear cloudy, and intact cells are in most areas hardly detectable, however, some intact nuclei as well as GFAP-positive astrocytic structures do appear. The cloudy appearance was likely due to cell debris remaining from the insufficient purification of the virus, as AAV9-NPC2-2A-GFP-P is the leftover product of the last cell debris clearing centrifugation step. The intact cells appeared to be mostly located in less cloudy areas of the wells, which could indicate that the cell debris clouds may have been detrimental to the cells.

The immunostainings of AAV9-NPC2-2A-GFP-S2 treated astrocytes illustrate a lack of cells throughout, as the cells evidently detached following the transduction. The observed cell detachment indicates that the treatment was noxious to the cells. However, it is unclear if the observed effect is due to the transduction by AAV9-NPC2-2A-GFP-S2 or if it is due to the fact that a higher volume of the AAV9-NPC2-2A-GFP-S2 solution was added due to the low titer (see *section 3.1.1*), only leaving room in the well for 40 % of the recommended amount of standard astrocyte culture medium.

Evident from immunostainings from both AAV9-NPC2-2A-GFP-P- and AAV9-NPC2-2A-GFP-S2 transduced cells is that no GFP-positive cells are detectable, which could imply low- to no infectivity of the AAV9-NPC2-2A-GFP-P and AAV9-NPC2-2A-GFP-S2 in the chosen concentrations. However, no definitive conclusions can be made on infectivity, as the appearance of cells was either very low or absent.

As AAV9-NPC2-2A-GFP-P, AAV9-NPC2-2A-GFP-S1 and AAV9-NPC2-2A-GFP-S2 appeared to be too contaminated by cell debris, or had a titer too low for proper transduction of primary cells, a decision was made to continue with AAV9-NPC2-2A-GFP provided by our laboratory, which had been purified by iodixanol gradient ultracentrifugation.

3.2 Infectivity of the provided AAV9-NPC2-2A-GFP

To investigate the infectivity of the provided AAV9-NPC2-2A-GFP, HeLa cells were treated with $4x10^9$ vg per well, and flow cytometry and ICC were performed. Results are illustrated in *figure 8.* Flow cytometry raw data is illustrated in *appendix 3*, and antibody controls can be found in *appendix 2.*

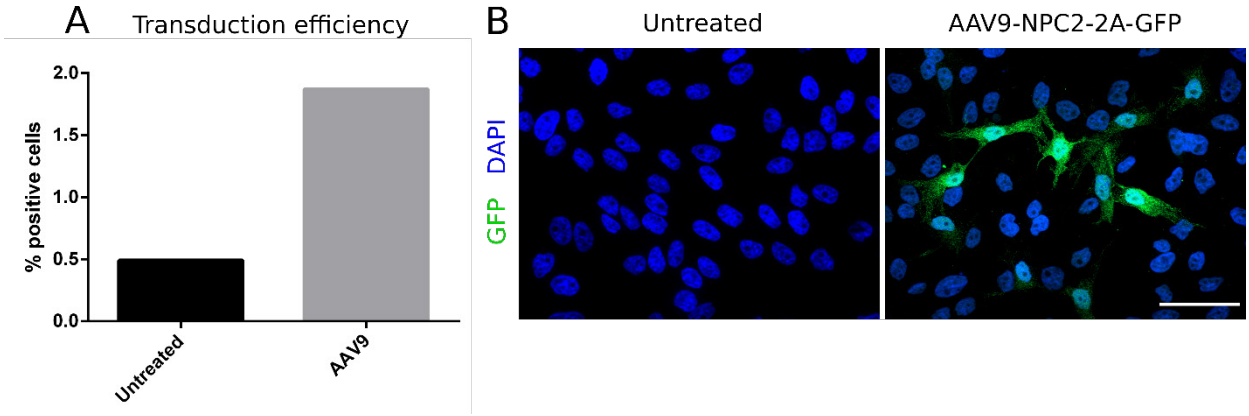

Figure 8: *Transduction efficiency of AAV9-NPC2-2A-GFP on HeLa cells (4x10⁹ viral genomes added per well).* ***A)*** *Flow cytometry showed a transduction efficiency of 1.87 % in the transduced cells (n=1). The rate for false positive transduction was gated at 0.49 % in the untreated cells (n=1).* ***B)*** *Representative immunofluorescent images of HeLa cells transduced with AAV9-NPC2-2A-GFP and untreated controls. Nuclei are stained with DAPI (blue). GFP-positive transduced cells shown in green. By visual inspection, it appears that immunostaining of GFP enhanced detection of transduced cells, as it is estimated that more than 1.87 % of cells are transduced in the immunostained images. Scale bar = 50 µm.*

As seen in *figure 8A*, 1.87% of the HeLa cells were detected as positive for the GFP tag compared to untreated cells. Based on this, it appears that the AAV9-NPC2-2A-GFP was infectious but had a low transduction efficiency. The low efficiency may be explained by fading of the GFP-tag and low expression of transgene, to which flow cytometry may not be sensitive enough to detect the fluorescence. This could partly be compensated for by immunostaining of the GFP-tag before flow analysis to enhance fluorescence intensity, thereby making it possible to detect positive cells with an otherwise weak fluorescence. Another factor that could have led to a low transduction efficiency could be if the titer of the sample was lower than expected (see *section 3.1.1* for a discussion of titer assays).

Immunostainings (*figure 8B*) supported the flow cytometry results, illustrating positively transduced HeLa cells by expression of the GFP-tag. Compared to the flow cytometry results, however, immunostainings illustrated what could appear to be a higher transduction efficiency by the number of cells visibly positive for GFP. As the GFP-tag was immunostained for fluorescence imaging, this would support the assumption that fading of the GFP-tag was partly the reason for the low transduction efficiency observed through flow cytometry.

In conclusion, AAV9-NPC2-2A-GFP has proven to be able to transduce HeLa cells as well as express its transgene, however, the exact transduction efficiency is unclear.

To evaluate if the findings in HeLa cells could be replicated in primary cells, monocultures of primary rat astrocytes were transduced with AAV9-NPC2-2A-GFP in a concentration of $5x10^9$- and 10^{10} vg per well, respectively. ICC was chosen as detection method, because it had proven to be the more sensitive method in HeLa cells (*figure 8*). Results are illustrated in *figure 9*.

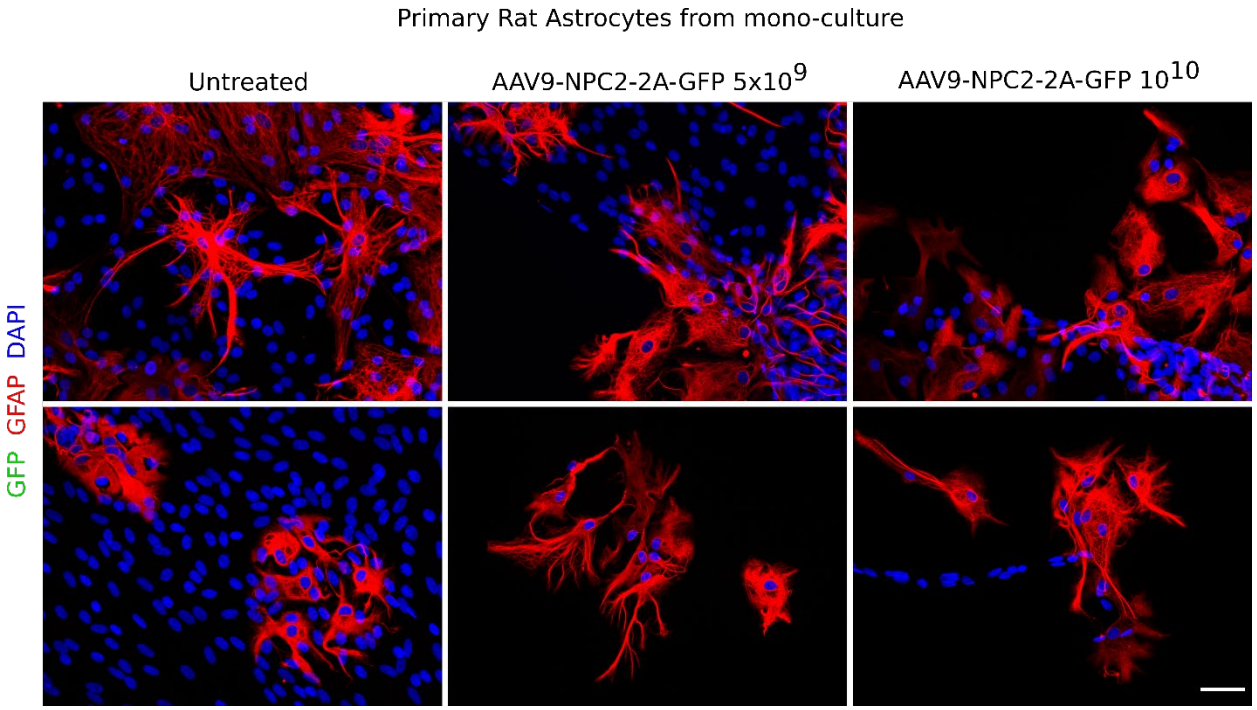

Figure 9: *Representative immunofluorescent images of primary rat astrocytes transduced with AAV9-NPC2-2A-GFP in concentrations of $5x10^9$- and 10^{10} viral genomes per well, respectively. Nuclei are stained with DAPI (blue). Astrocytic GFAP expression is shown in red. GFP was expected to show in green, but could not be detected, indicating that no astrocytes were transduced. Addition of AAV9-NPC2-2A-GFP appears noxious to astrocytes, evident by the cellular detachment, and reactive remaining astrocytes. Scale bar = 50 µm.*

Based on immunostainings, the positive transduction results in HeLa cells could not be replicated in primary rat astrocytes, as no GFP-positive cells could be detected for neither the concentration of $5x10^9$, nor 10^{10} vg per well (see *figure 9*). These findings implicate that either the astrocytes were not transduced by AAV-NPC2-2A-GFP, or the transgene was not expressed properly in the astrocytes to be detectable, i.e. viral entry may never have taken place, the genome may lie latent, or the virion could have been degraded in lysosomes before even reaching the nucleus (see *figure 2* for an illustration of the intracellular pathway of AAV9). Another possibility is that some astrocytes were transduced, but that it had a detrimental effect on the cells, causing them to detach, explaining the near-empty coverslips in transduced wells. Though no positively transduced cells were detected, the addition of AAV9-NPC2-2A-GFP clearly affected the primary rat astrocytes. In many areas of the wells, only small clusters of GFAP-positive astrocytes appeared, and cells that were not GFAP-positive appeared to be mostly attached to the GFAP-positive astrocytes, and not the wells.

These findings are very different from the findings in the transduced HeLa cells, which did not appear to be affected by the AAV-NPC2-2A-GFP in a detrimental way (*figure 8B*). HeLa cells are well-known to be a robust cell line [121], which could explain the discrepancy. Moreover, primary rat astrocytes and HeLa cells are vastly different cell types, as well as from different species, which may also explain the inconsistency regarding GFP-expression.

A possible explanation as to why HeLa cells were more receptive to AAV9-NPC2-2A-GFP transduction than astrocytes may be if the vector was defective in its VP1-region. As the sequence of the *rep/cap* plasmid, pAAV9, used in the current study is unknown, it opens up the possibility that it may be mutated in places, such as in the VP1-region, which could result in dysfunctional capsid proteins, thereby reducing functionality of the finished product (the importance of a functional virion structure can be deducted from *figure 2*). VP1 has been found to be crucial for endosomal escape [95,96], and a defect would thereby prevent proper transduction in most cell types. However, others have found that HeLa cells can take up a small fraction of a VP1-defective vector, which in theory should all accumulate in

the perinuclear region [120]. It was hypothesized that because HeLa cells divide so frequently, the nuclear membrane may have been somewhat permeable at times of cell division, allowing non-infectious vectors to reach the nucleus by circumstantial factors more so than factors related to its capsid [120]. Had the virion been functional, it ought to be able to transduce astrocytes, considering what others have found both in vivo and in vitro [80,122,123].

In any case, based on the collective results from transduction of HeLa cells and primary rat astrocytes, respectively, the AAV9-NPC2-2A-GFP appeared to be functional and infectious in HeLa cells, however, the effect could not be reproduced in primary astrocytes, and may be limited to rapidly dividing cell lines. It cannot be ruled out that the vector may be functional in different cell types or tissues, but its infectious effectivity appeared limited overall.

3.3 Effects of the provided AAV9-NPC2-2A-GFP on the in vitro BBB model

To investigate the effects of AAV9-NPC2-2A-GFP in a setup more similar to in vivo conditions than monocultures, an astrocyte-endothelial cell non-contact co-culture BBB model was set up and transduced with AAV9-NPC2-2A-GFP in a concentration of $5x10^9$ vg per filter.

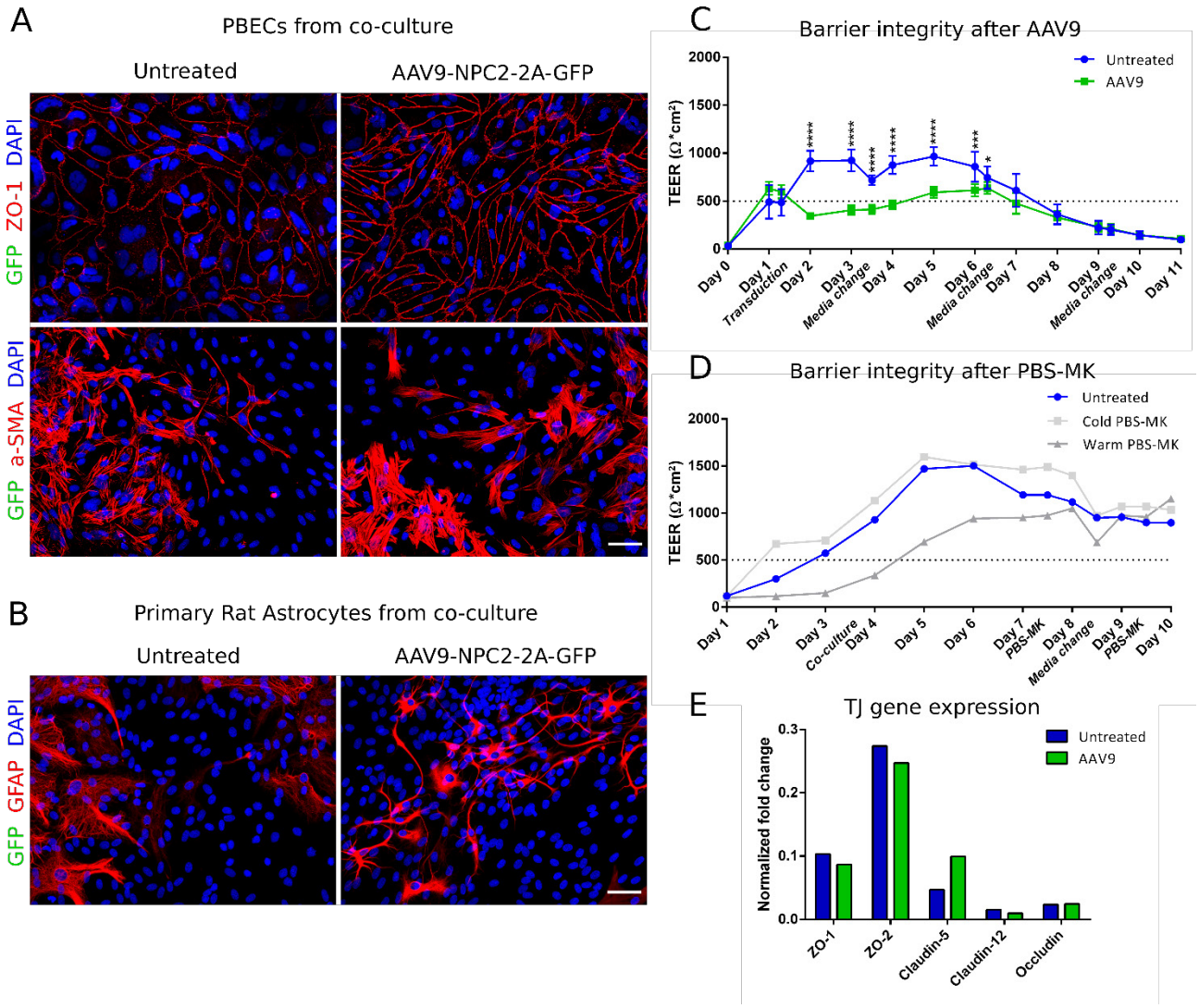

Figure 10: *Results from a primary rat astrocyte and porcine brain endothelial cell (PBEC) non-contact co-culture BBB model treated with AAV9-NPC2-2A-GFP.* ***A)*** *Representative immunostainings of the PBECs transduced with AAV9-NPC2-2A-GFP ($5x10^9$ viral genomes (vg) per filter). Nuclei are stained with DAPI (blue). Endothelial ZO-1 expression and pericytic α-SMA expression are shown in red. GFP was expected to show in green, but was not detectable, indicating no cells were transduced. Scale bar = 50 µm.* ***B)*** *Representative immunostainings of primary rat astrocytes from the co-cultures transduced with AAV9-NPC2-2A-GFP ($5x10^9$ vg per filter). Nuclei are stained with DAPI (blue). GFP was expected to show in green, but was not detectable, indicating that no successful transduction had taken place. Astrocytic GFAP expression is shown in red. Astrocytes appeared more reactive in the AAV9-treated wells. Scale bar = 50 µm.* ***C)*** *TEER measurements from the co-cultures transduced with AAV9-NPC2-2A-GFP*

*(5x10⁹ vg per filter) (n=9) and untreated controls (n=9). TEER data is depicted as Ω/cm²± standard deviation. TEER values drop rapidly after addition of AAV9, causing significantly lower TEER values compared to the untreated controls from day 2 to day 6, indicating that the virus impaired barrier integrity. *p<0.5, ***p<0.001, ****p<0.0001.* ***D)*** *TEER measurements from a co-culture BBB model treated with cold PBS-MK (n=1), warm PBS-MK (n=1), and an untreated control (n=1). TEER data is depicted as Ω/cm²± standard deviation. Dotted line depicts the TEER value at which the PBECs are permeable to mannitol. The PBS-MK solutes do not appear to elicit a drop in TEER.* ***E)*** *qPCR investigation of tight junction proteins ZO-1, ZO-2, Claudin-5, Claudin-12 and Occludin on AAV9-NPC2-2A-GFP-transduced PBECs (5x10⁹ vg per filter) (n=1) and untreated PBECs (n=1). Dotted line depicts the TEER value at which the PBECs are permeable to mannitol. Normalized fold change for Claudin-5 was twice as high in AAV9-treated PBECs, but no conclusions can be drawn due to a lack of replicates.*

3.3.1 GFP-expression

Immunostainings were performed on PBECs and primary rat astrocytes from the in vitro BBBs to investigate if the cells were efficiently transduced by the AAV9-NPC2-2A-GFP (see *figure 10A* for immunostainings of PBECs, and -*10B* for immunostainings of primary rat astrocytes). The GFP-staining was undetectable in both cell types, indicating that either the PBECs and primary rat astrocytes were not transduced by the AAV9-NPC2-2A-GFP, or the transgene was not expressed properly in the cells to be detectable. To further investigate if AAV9-NPC2-2A-GFP had transduced the barriers, the more sensitive method, RT-qPCR, was performed on RNA harvested from the primary rat astrocytes and PBECs with a primer targeting the transgenic GFP. Although the RT-qPCR results cannot be considered reliable, because of non-optimal primer efficiency, they did suggest that no transgene was expressed in the transduced cells, supporting findings in immunostainings (elaborated upon in *appendix 5)*. It was speculated that a co-culture, being marginally closer to in-vivo situations, may be different than astrocyte monocultures in regards to susceptibility to transduction (see *figure 9* and *section 3.2*), but these results demonstrated that the AAV9 used in this study was non-infectious in a primary cell based in vitro BBB model as well. It appears increasingly evident that it will pose a challenge to utilize this vector in cells very unlike HeLa cells (for a more elaborate discussion, see *section 3.2*).

3.3.2 Indirect effects of AAV9-NPC2-2A-GFP

Immunostainings on the PBECs and primary rat astrocytes were also used to investigate if AAV9-NPC2-2A-GFP could have a detrimental effect on the cells (see *figures 10A* and *10B*).

In regard to cell morphology, astrocytes in co-culture treated with AAV9-NPC2-2A-GFP appeared more reactive than controls, which was evident by their elongated processes with a strong, but condensed expression of GFAP. This was in contrast to the untreated cells which had a more diffuse, veil-like expression of GFAP (*figure 10B*).

Interestingly, the junctional complexes between PBECs did not appear to be perniciously affected by the addition of AAV9-NPC2-2A-GFP based on their expression of ZO-1 (*figure 10A*), which appeared tight and cell-confining. If ZO-1 had been compromised, gaps would be observed in the ZO-1 staining, or it would appear as parallel double structures, rather than a united line, indicating paracellular empty space (L.B. Thomsen, unpublished). The effects of AAV9-NPC2-2A-GFP on ZO-1 was also investigated via qPCR (depicted in *figure 10E*), and from these results, it can be cautiously stated that no change in gene expression of ZO-1 was observed either. If it was the case that ZO-1 was upregulated, it might also show in immunostainings as perinuclear diffuse stainings projecting towards the cell border (L.B. Thomsen, unpublished), which was not observed either (*figure 10A*). However, as cells were fixed for immunostainings and mRNA was harvested at the end of the experiment (day 11, *figure 10C*), it is uncertain whether this is a true reflection of ZO-1 expression throughout the culture period. Importantly, TEER increased in AAV9-treated barriers following the decrease (a steady incline is seen from day 2 to day 6, *figure 10C),* and by day 10, where the cells were harvested, TEER values were fully comparable between culture conditions. If cells had been harvested on day 2 or 3, there might have been changes to observe in the ZO-1 expression of AAV9-treated barriers.

It can be speculated that the virus may have transcytosed the PBECs, based on the overall observation that astrocytes in the bottom chamber appear more affected by the treatment. Because this study was not able to track the viral vector by its transgene expression, this remains a hypothesis based on previous findings that AAV9 is able to cross BECs by transcytosis [80]. Besides, it cannot be dismissed that AAV9 may have crossed the PBECs by paracellular diffusion, as the drop in TEER indicates that the barrier was more permeable in the first days after AAV9 addition. To elucidate this, the study would benefit from stainings of PBECs fixed the day after transduction, preferably including stainings of Occludin and claudins, e.g. Claudin-5, as their positioning in the intercellular cleft [40] may be better indicators of whether paracellular transport has been facilitated or not. Furthermore, a permeability assay would provide addition insight into the likelihood of paracellular diffusion through the PBECs, as the cut-off TEER value of 500

(*figure 10C*) is based on permeability of mannitol, which is likely more miniscule in diameter compared to AAVs (18-26 nm).

3.3.3 Compromised barrier integrity

While ZO-1 expression did not appear to be compromised at day 10 post transduction, it is evident that barrier integrity has been affected by addition of AAV9-NPC2-2A-GFP, regardless, based on the TEER measurements that were obtained throughout the culturing, which can be seen in *figure 10C*. The results show a rapid drop in TEER following the transduction on day 1, while the TEER values of untreated barriers increase as expected. The decrease in TEER for AAV9-NPC2-2A-GFP treated barriers is observed until day 2, where it is significantly lower than TEER in untreated barriers. From day two, TEER values of AAV9 treated barriers appear to increase slowly but remain significantly lower than the controls until day 6 after which they normalize, and from day 8 they correspond to the untreated barriers. Because of the rapid decrease, followed by a slow increase in TEER, it could be speculated that the AAV9-NPC2-2A-GFP transduction may have shocked the cells, after which they slowly recovered.

Though the effects of AAV9-NPC2-2A-GFP treatment on the barrier integrity were evident, it is unclear specifically what the drop in TEER may be attributed to. One factor thought to affect TEER in in vitro BBB models is pericyte growth in the filter inserts (L.B. Thomsen, unpublished), which was observed in the current PBEC cultures by the α-SMA positive structures (*figure 10A*). The presence of pericytes on the opposing side of the cell culture filter insert with BECs has been shown to support BBB integrity, corresponding with the anatomical arrangement in cerebral microvessels [124]. Indeed, the presence of pericytes on the basolateral side of BECs has been shown to be important for the proper apicobasal polarization [125]. Thus, it can be speculated that the presence of pericytes intertwined with the PBECs comparable to the luminal side (*figure 10A*) may have skewed polarization, hence contributing to the decreasing barrier integrity. However, as this was the case for both AAV9-NPC2-2A-GFP treated and untreated barriers, it is unlikely to have caused to the rapid decrease in barrier integrity in virus-treated barriers (*figure 10C*).

In an effort to rule out the possibility that thinning of the media by addition of the AAV9-NPC2-2A-GFP solution caused the sudden decrease in barrier integrity, barriers were set up, testing the effect of 1X PBS-MK on TEER measurements, which corresponded to the PBS-MK content in the vehicle, in which AAV9-NPC2-2A-GFP was dissolved (results can be seen in *figure 10D*). In addition to PBS-MK, the viral solution contained iodixanol, but as this was not accessible, a proper control vehicle could not be prepared. Since TEER measures the electrical resistance [109], slight alterations in ionic balance may have affected measurements, but iodixanol is non-ionic and non-toxic [126], and thus it may suffice to conduct a test using PBS-MK corresponding to the ionic content and volume of the AAV9-NPC2-2A-GFP vehicle. Because temperature is known to influence TEER measurements [109], and the virus had been stored at 4℃ prior to addition to the barriers, it could be speculated that a temperature shock may have influenced measurements as well. This was investigated by addition of cold PBS-MK, which was compared against lukewarm PBS-MK and an untreated control.

Based on the TEER measurements illustrated in *figure 10D*, the PBS-MK solute does not appear to affect barrier integrity, neither after the treatment on day 7, nor after the treatment on day 9. This makes it increasingly likely that the drop in TEER seen in the AAV9-NPC2-2A-GFP treated barriers can be attributed to the virus itself (*figure 10C*).

3.3.4 AAV9-NPC2-2A-GFP effects on TJ proteins

In an effort to further elucidate the effect of AAV9-NPC2-2A-GFP on barrier integrity, gene expression on a wider range of TJ proteins was investigated on the PBECs; ZO-2, Claudin-5, Claudin-12 and Occludin, in addition to the ZO-1 mentioned in *section 3.3.2* (illustrated in *figure 10E*). Based on these results, AAV9-NPC2-2A-GFP does not appear to have affected the transcriptional gene expression of ZO-2, Claudin-12 or Occludin either. However, the normalized fold change of Claudin-5 was twice as high in AAV9-NPC2-2A-GFP transduced PBECs compared to the control (*figure 10E*). Worth noting is that the TEER measurements in the current study indicate that barrier integrities were alike between transduced- and untreated barriers at day 10 post-transduction, where mRNA was harvested (see *figure 10C*), hence it could be speculated that gene expression may partly be normalized at this point. To investigate the immediate effect of transduction with AAV9-NPC2-GFP, it may thus be preferable to harvest the mRNA much sooner, i.e. at 24-120 h post-transduction, where a significant effect is observed in TEER measurements (*figure 10C*).

However, worth discussing is that the expression of Claudin-5 has been found to be modulated by acute insult in several neurological disease models, illustrating a pattern of decreased Claudin-5 expression 24 h post-induction, followed by an increased expression 48 h and 72 h post-induction [127–129] . It could be speculated that the Claudin-5 expression in the current study may have followed a similar pattern after addition of the virus, thereby explaining the

increased expression. It is, however, unfeasible to make a direct comparison, as the results of the current study were obtained 10 days post-transduction, and the cause of insult to the BBB in the current study varies from the previous studies [127–129].

As such, no definite conclusions can be drawn from these results; the setup needs to be repeated to get a number of replicates sufficient for statistical analysis, but our preliminary analysis indicate that there might be changes to be seen in Claudin-5 expression with further investigations.

3.3.5 Safety concerns to using AAV9 as a therapy

BECs, as well as surrounding cell types, such as microglia, pericytes and astrocytes, are considered to produce pro-inflammatory cytokines, as a result of neurotropic viral infection of the CNS [130]. These pro-inflammatory cytokines are conceived to enhance diapedesis, in part by modulation or degradation of TJ proteins, as a mean to enhance leukocyte transport into the CNS [131,132]. Thereby, the BBB integrity would be lowered, which presents itself as diminished TEER values in BBB models [131,132]. As the results of the current study show a decrease in TEER after addition of virus, a possible change in expression of Claudin-5, as well as astrocytic reactivity, it can be speculated that a similar process has occurred. If AAV9 does cause a change in expression of Claudin-5, and does indeed induce diapedesis, allowing infiltration of immune cells, it poses a potential safety concern to the use of AAV9 as a therapy. As mentioned in *section 1.2*, the tightness of the BBB is protective for the CNS in terms of shielding the brain from invading pathogens and other harmful substances, and the rapid drop observed in TEER could be detrimental in vivo. Naturally, these issues must be further investigated before we deem them a factual concern; for now, they remain speculations.

Unfortunately, this is not the only possible safety concern to rAAV based gene therapies, as they come with a risk of viral integration into the genome. A latent infection with the wild type AAV has been associated with integration into the AAVS1 integration site on the long arm of chromosome 19 (19q13-qter) due to its Rep protein (a DNA helicase) [133–135]. Fortunately, this site-specific integration does not occur with the recombinant vectors [73] used for tailored gene therapy, because rAAVs are normally produced to be devoid of the rep gene, as it is instead provided in trans [112]. However, it is worth noting that rAAVs can also integrate into the genome in other sites of the genome in a *rep*-independent non-random fashion, e.g. preferentially into ribosomal RNA repeats, satellite DNA and palindromic DNA [73], and it may pose a safety concern to rAAV gene therapy. In fact, a heightened risk of hepatocellular carcinoma has been observed in mice after systemic injection [70–72], but this has not yet been reported in humans [67]. Though there is a risk of viral integration into the genome, it is largely agreed that the rAAV genomes predominantly remain episomal [73,74], and may therefore be advantageous compared e.g. to lentivira. Furthermore, it may be worth the trade-off if the effects are stable, sustained gene expression, providing therapeutic levels of secreted protein.

3.4 Therapeutic potential of AAV9-NPC2-2A-GFP

An ELISA for quantitative detection of NPC2 was performed on conditioned media from AAV9-NPC2-2A-GFP-transduced co-culture barriers, to evaluate the therapeutic potential of AAV9-NPC2-2A-GFP through increased production of NPC2.

Sample condition	**pg/mL**
Untreated, upper chamber	Not detectable
Untreated, lower chamber	244
AAV9-NPC2-2A-GFP-transduced, upper chamber	Not detectable
AAV9-NPC2-2A-GFP-transduced, lower chamber	Not detectable

Table 6: *NPC2 ELISA results on pooled conditioned medium from 9 upper- and 9 lower chambers, from AAV9-NPC2-2A-GFP-transduced and untreated barriers (n=1), analyzed in duplicates. Mean absorbance and NPC2 concentrations are depicted after subtraction of mean zero standard absorbance. Secreted NPC2 was undetectable in all conditions with the exception of the untreated lower chamber.*

Based on the ELISA results, listed in *table 6*, no conclusions can be made regarding the therapeutic potential of AAV9-NPC2-2A-GFP, as concentrations of NPC2 protein in the majority of the samples were lower than the minimum

detectable dose of the kit (>156.25 pg/ml). Only medium from the lower chamber of an untreated barrier showed a detectable dose of NPC2 (244 pg/mL). As the cells used to create the co-culture BBB model are wild-types and not NPC-mutants, the detectable amount of NPC2 present in the untreated lower chamber, likely represents their endogenous production of NPC2.

From visual inspection, the untreated astrocytes seemed more viable than the AAV9 treated astrocytes (*figure 10B*), which may account for the detectable amount of NPC2 production in the untreated cells. It could be speculated that the undetectable amount of NPC2 in medium from AAV9 treated cells is due to a decreased cell viability. As NPC2 levels are undetectable, it is unlikely that the AAV9 treated cells express the NPC2 transgene, supporting observations from immunostainings and RT-qPCR (*figure 10B and appendix 5*). As the range of the ELISA kit was approximately 156.25 pg/mL to 10,000 pg/mL, the concentration of NPC2 in the untreated lower chamber lies in the lower range, and the study would consequently need to be repeated, before any conclusions should be drawn. For proper investigation, an ELISA kit with a lower minimum detectable dose of NPC2 should be employed.

3.5 Optimization of detection of AAV9-NPC2-2A-GFP

Choice of promoter upstream of the transgene can influence transgenic expression [123,136,137]. Thus, to ensure that the CAG promoter, present in the AAV9-NPC2-2A-GFP genome, is effective in initiating transcription of the transgene, a transfection study was performed in HeLa and bEnd.3 cells comparing CAG to an alternative promoter; the CMV. As elaborated in *appendix 6*, cloning of a pCMV-NPC2-2A-GFP plasmid did not succeed. Instead the pFastbac-AAV-CAG-NPC2-2A-GFP was compared to the CMV-EPO-GFP plasmid, as both plasmids contain the same fluorescent tag downstream of their respective promoters. The transfection efficiencies were compared by ICC and flow cytometry and results are presented in *figure 11*.

When looking at the fluorescence images (*figures 11A-B*), both immunostainings of NPC2 and EPO, respectively, colocalized with the GFP, confirming transfection with the two different plasmids. However, small amounts of immunostained EPO is observed in untreated cells, and in some of the transfected cells not expressing GFP, indicating an endogenous expression of this hormone. Thus, the transfection efficiency should only be counted by the presence of the transgenic GFP. GFP positive cells were observed in both HeLa and bEnd.3 cells after transfection with both plasmids. It did, however, appear that more pCAG-NPC2-2A-GFP transfected cells were GFP-positive compared to the pCMV-EPO-GFP transfected cells, especially when compensating for total number of nuclei.

Comparing fluorescence images (*figures 11A-B*) to flow cytometry (*figures 11C-D*) for both HeLa- and bEnd.3 cells, the observed ratio of transfected cells in fluorescence images does not quite equate to the higher ratio measured by flow cytometry (97% and 68% in HeLa cells, and 13% and 6% in bEnd.3 cells). This may be explained by a variation in the intensity of transgene fluorescence between cells. Flow cytometry compensates for this by measuring all intensities, and categorizes the cell as positive, when the fluorescence is more intense than the untreated cells. In contrast, fluorescent images are more limited in displaying all intensities, meaning that some positive cells may not be visible at the selected exposure setting.

In this experiment, GFP was not immunostained for fluorescence images, which could help explain why transfection efficiency appears lower on the images than flow cytometry, which was in contrast to the results on transduced HeLa cells (*section 3.2*), where transduction efficiency appeared higher in GFP-immunostained images than flow cytometry. The quantitative information given from flow cytometry in this experiment is considered valid, although immunostainings may not correlate completely. Raw data from flow cytometry is depicted in *appendix 7.*

In flow cytometry results from HeLa cells, transfection appeared to be more efficient in the pFastbac-CAG-NPC2-2A-GFP transfected cells, compared to the pCMV-EPO-GFP transfected cells (*figure 11C*). The flow cytometry experiment was repeated twice in bEnd.3, to investigate if the same pattern presented in cells more reminiscent of BECs. In bEnd.3 cells, significantly more positive pFastbac-CAG-NPC2-2A-GFP transfected cells (n=6) were detected, compared to pCMV-EPO-GFP positive cells (n=6) (*figure 11D*). This could be due to a higher ratio of the positively transfected cells being detected, because of a stronger GFP signal, if the CAG promoter is more active compared to the CMV promoter. Another reason for the unequal transfection efficiency may be differences between plasmids regarding e.g. size and sequence.

An important factor to take into consideration, is that pFastbac-CAG-NPC2-2A-GFP includes a Woodchuck Hepatitis virus posttranscriptional regulatory element (WCE) and pCMV-EPO-GFP does not. WCE has been observed to increase transgene expression, by helping intronless RNA leave the nucleus and by protecting promoters against silencing [138]. The CAG promoter includes introns and is less dependent on WCE, but the CMV promoter is intronless, making this element important for optimal activity of this promoter [138]. Thus, WCE can be speculated to influence the transcriptional expression of the transgene and the observed differences between pFastbac-CAG-NPC2-2A-GFP and

pCMV-EPO-GFP transfection efficiency in this experiment. A more valid comparison could be made between two plasmids, both containing the WCE, as originally planned with the cloned pCMV-NPC2-2A-GFP vs. the pFastbac-CAG-NPC2-2A-GFP.

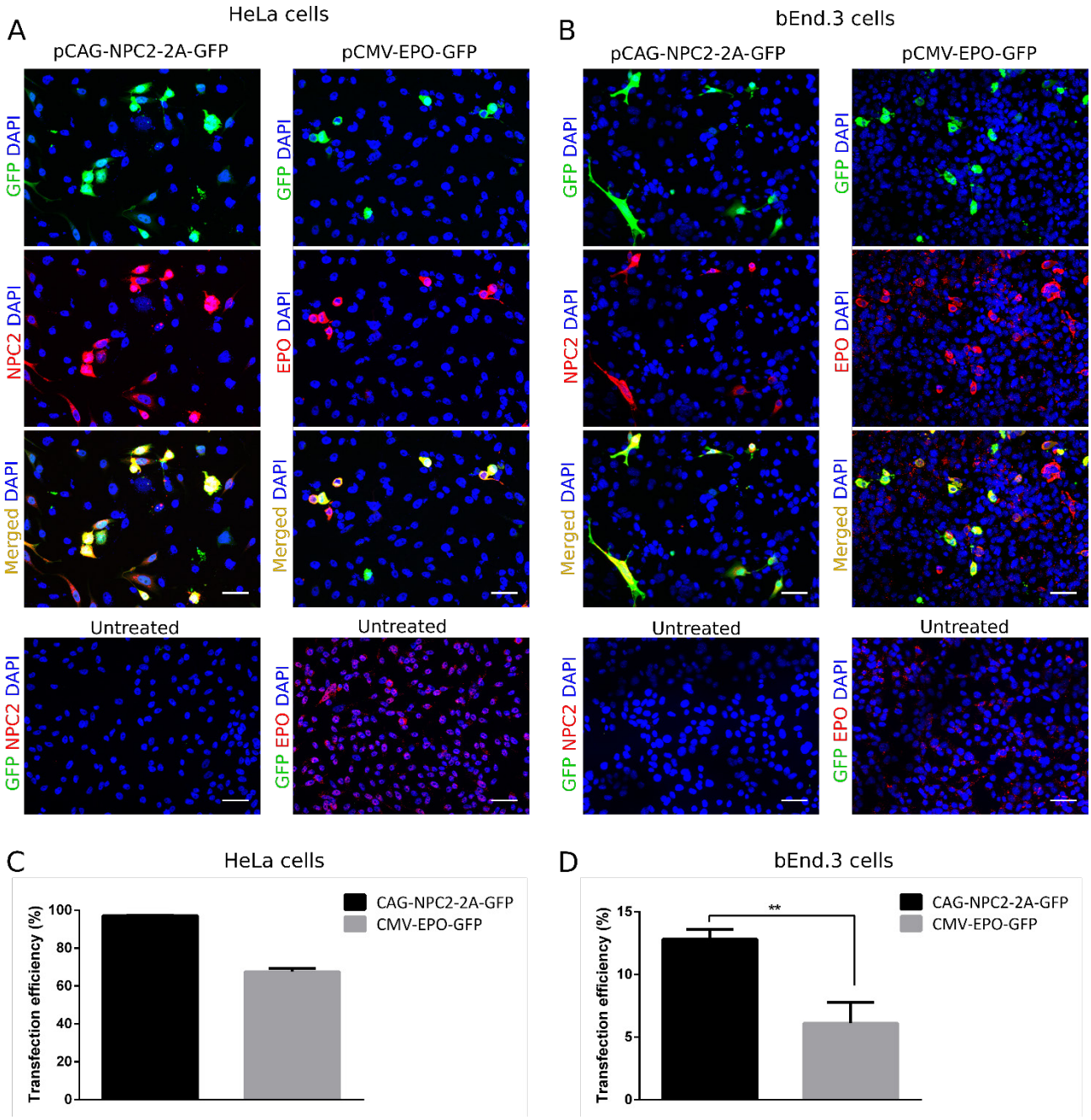

***Figure 11**: Comparison of the detected transfection with either pFastbac-CAG-NPC2-2A-GFP or pCMV-EPO-GFP in HeLa and bEnd.3 cells. **A-B)** Representative fluorescent images of transfected and untreated HeLa cells (A) and bEnd.3 cells (B) with the transgenic GFP tag observed in green, and immunostainings of NPC2 and EPO, respectively, in red. Nuclei are stained with DAPI (blue). The GFP tag is observed to colocalize with both NPC2 and EPO stainings, visualizing transgene expression. However, EPO appears to be expressed in cells lacking GFP-expression as well, and in untreated cells, indicating endogenous expression of EPO. In both HeLa- and bEnd.3 cells pCAG-NPC2-2A-GFP transfected cells appear more GFP positive compared to pCMV-EPO-GFP transfected cells, when standardized to total number of nuclei. Scale bar = 50 µm. **C)** Transfection efficiency in HeLa cells measured with flow cytometry. HeLa cells transfected with pFastbac-CAG-NPC2-2A-GFP (n=2) appeared to have higher transfection efficiency (97%) compared to those transfected with pCMV-EPO-GFP (n=2) (68%). Untransfected cells (n=2) were used to set the gate for positively transfected cells from GFP fluorescence, allowing a false positive rate of <0.5%. Examples of raw*

data is presented in appendix 7. ***D)*** *Transfection efficiency in bEnd.3 cells measured with flow cytometry showed the same pattern as in HeLa cells. BEnd.3 cells transfected with pFastbac-CAG-NPC2-2A-GFP (n=6) showed a significantly higher transfection efficiency (mean 12.87% ± SD 0.79) compared to bEnd.3 cells transfected with pCMV-EPO-GFP (n=6) (mean 6.11% ± SD 1.69). **p<0.01. Untransfected cells (n=6) were used to set the gate for positively transfected cells from GFP fluorescence, allowing a false positive rate of <0.5%. Examples of raw data is presented in appendix 7. Collectively, the results suggest that more cells were transfected with pCAG-NPC2-2a-GFP than pCMV-EPO-GFP, or alternatively, that cells were transfected equally with the two plasmids, but because of higher activity of the CAG promoter, more transgene expression can be observed in these cells.*

The CMV promoter originates from cytomegalovirus' immediate-early enhancer- and promoter sequences, and is considered a strong promoter for mammalian cells with ubiquitous activity [138]. The CAG promoter is a synthetic promoter, designed by combining the enhancer sequence from CMV with parts of the chicken β-actin gene, along with a fragment of the rabbit β -globulin gene [136,139], which together makes a very strong promoter, with ubiquitous activity [138]. Several studies have made comparisons of promoters including CAG and CMV, however, their activity varies between species, tissue type and in vitro/in vivo studies. One study found CMV to be more effective than CAG in mouse embryonic spinal cord cultures [123]. An in vivo study on lentiviral vector delivered to CNS in rats and monkey, found that CAG promoter had much higher activity than CMV in rat glial cells, but more equal activity in monkey glial cells [140]. An in vivo study with AAV delivery of transgene to mice and rats cochlea cells found CAG promoter to be more active than the CMV promoter [137]. Collectively, these studies highlight the importance of testing promoter efficiency in the specific target species and cell type of the experiment.

Although it is tempting to suggest that the difference between transfection efficiency observed in this experiment is due to the CAG promoter being more active than the CMV promoter, investigation of several steps in the pathway between transfection and protein expression needs to be elucidated in order to make the final conclusion. A relevant perspective could be quantification of transgene DNA located inside the cells by qPCR, based on purified DNA. This would provide a more direct measure of transfection efficiency. Furthermore RT-qPCR on purified mRNA could provide a direct measure of transcriptional expression of the transgene, and thus a direct measure of promoter efficiency, especially when normalized to the transgene DNA levels. Finally, comparing two plasmids with more similar sequences besides the promoter, would increase reliability of the experiment.

3.6 Luciferase assay as an optimized detection method

A luciferase assay was performed, comparing HBMEC, HeLa-, bEnd.3- and RBE4 cells transfected with plasmid DNA encoding firefly luciferase, to evaluate the sensitivity of the luciferase assay, and whether the assay could potentially be applied to detection of AAV9 transduction in the future. Results are illustrated in *figure 12*.

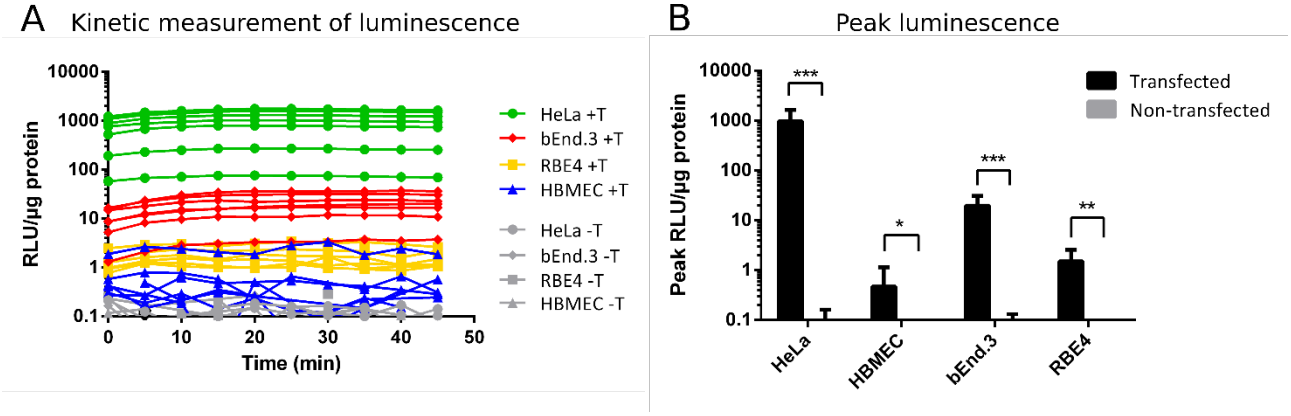

Figure 12: *Transfection efficiency in HeLa cells (n= 7), HBMEC (n= 7), bEnd.3 cells (n= 7) and RBE4 cells (n= 7) transfected with pFastbac-CAG-Luciferase, measured by a luminescence assay and normalized to a BCA assay.* ***A)*** *Kinetic measurements of emitted light produced by the transgenic luciferase over 45 min after adding the luciferin substrate, normalized to total protein concentrations. Transfected HeLa cells (green) are expressing very high levels of luminescence, indicating a higher transfection efficiency compared to the transfected endothelial cell lines, of which transfected bEnd.3 cells (red) appears to have the highest transfection efficiency. Untreated cells (grey) express luminescence levels close to zero, lower than any of the transfected cells. It appears that luminescence peaks approximately at 20 min after addition of luciferin.* ***B)*** *Luminescence normalized to protein levels at 20 min post luciferin addition were analyzed by multiple Mann-Whitney non-parametric tests, revealing significant*

*differences between transfected (n=7) and untreated cells (n=7) in all 4 cell types. *p<0.5, **p<0.01, ***p<0.001. From this experiment, it appears that the luciferase assay is a sensitive method, able to detect modest levels of transfection (i.e. transfected HBMEC), and specific, as it can clearly differentiate between different levels of transfection i.e. HeLa vs. RBE4. However, it can only do relative comparisons between samples, and not quantify the exact ratio of positively transfected cells, like flow cytometry.*

The kinetic measurements of the luciferase assay (*figure 12A*) illustrate very high levels of luminescence from transfected HeLa cells, indicating a higher transfection efficiency compared to the transfected endothelial cell lines. This corresponds with the results in *section 3.5*, also illustrating higher transfection efficiency in HeLa cells, compared to bEnd.3 cells. The bEnd.3 cells, however, appear to have the highest transfection efficiency of the endothelial cell lines, followed by the RBE4 cells and finally HBMEC. Luminescence normalized to protein levels at 20 min following luciferin addition were analyzed and revealed significant difference between transfected and untreated cells in all four cell lines (*figure 12B*).

From this experiment, it appears that the luciferase assay is a sensitive method which is able to detect even modest levels of transfection (i.e. transfected HBMEC), and a specific assay as it can differentiate clearly between transfection efficiency in the different cell lines. Furthermore, it was established that it is feasible to measure the luminescence on trypsinized cells (data not shown), which had been moved to an opaque well plate, making it possible to assess cells from a co-culture. This makes the luciferase assay equal in practicality to e.g. flow cytometry. However, it is only possible to make relative comparisons between samples in luciferase assays, rather than quantifying the exact percentage of positively transfected cells, like flow cytometry, which is a limitation of the method.

Based on the sensitivity of the assay, it is indicative that luciferase assays might be an applicable assay for detecting transduction efficiency as well as transfection efficiency, even if the efficiencies are at a low range. However, further studies on AAV9-luciferase transduced cells are necessary to confirm this.

4. Conclusion

The aim of this study was to produce AAV9-NPC2-2A-GFP, to evaluate it as a novel therapeutic strategy for treatment of NPC2 disease. It was hypothesized that AAV9 viral vectors could transduce and genetically modify in vitro BBB models and induce NPC2 protein secretion, without compromising the BBB integrity. Based on the results, the AAV9 viral vector could not successfully transduce or genetically modify the in vitro BBB models, and a therapeutic potential could not be demonstrated. Furthermore, the AAV9 treatment appeared to have a detrimental effect on the BBB, as this study observed a rapid decrease in TEER following AAV9 treatment, indicating compromised integrity of the barrier. Moreover, astrocytes in the BBB model appeared more reactive following AAV9 treatment, contributing to the perception of AAV9 treatment being detrimental to the BBB.

On the basis of this study, AAV9 does not appear suitable as a novel therapeutic strategy for treatment of NPC2 disease, however, this may be attributed to a lack of functionality of the current vector, as it contrasts with the potential of AAV9 seen in other studies, hence further investigations are necessary to make any final conclusions.

In the additional optimization study, it was found that the transfection efficiency was superior when HeLa and bEnd.3 cells were transfected with plasmids containing CAG promoter, compared to plasmids containing the CMV promoter. However, further study is necessary to make any conclusions on the general potential of the promoters to modulate transgene expression. Beyond that, a luciferase assay was evaluated to be an applicable, sensitive assay for detection of transfection, however, no conclusions could be made in regards of applicability for detection of transduction efficiency.

5. References

1. Naureckiene, S. *et al.* Identification of HE1 as the second gene of Niemann-Pick C disease. *Science (80-.).* **290,** 2298–2301 (2000).
2. Carstea, E. D. *et al.* Niemann-Pick C1 Disease Gene: Homology to Mediators of Cholesterol Homeostasis. *Science (80-.).* **277,** 228–231 (1997).
3. Bi, X. & Liao, G. Cholesterol in Niemann-Pick Type C disease. *Subcell. Biochem.* **51,** 319–335 (2010).
4. Wassif, C. A. *et al.* High incidence of unrecognized visceral/neurological late-onset Niemann-Pick disease, type C1, predicted by analysis of massively parallel sequencing data sets. *Genet. Med.* **18,** 41–48 (2016).
5. Sleat, D. E. *et al.* Genetic evidence for nonredundant functional cooperativity between NPC1 and NPC2 in lipid transport. *Proc. Natl. Acad. Sci.* **101,** 5886–5891 (2004).
6. Winstone, A. M., Stellitano, L. A. & Verity, C. M. Niemann–Pick type C as a cause of progressive intellectual and neurological deterioration in childhood. *Dev. Med. Child Neurol.* **59,** 965–972 (2017).
7. Imrie, J., Heptinstall, L., Knight, S. & Strong, K. Observational cohort study of the natural history of Niemann-Pick disease type C in the UK: A 5-year update from the UK clinical database. *BMC Neurol.* **15,** (2015).
8. NPC intracellular cholesterol transporter 2 (Homo sapiens). at: https://www.ncbi.nlm.nih.gov/gene/10577 (Accessed: 30th May 2019)
9. Kirchhoff, C. Molecular cloning and characterization of HE1, a major secretory protein of the human epididymis. *Biol. Reprod.* **54,** 847–856 (1996).
10. Willenborg, M. *et al.* Mannose 6-phosphate receptors, Niemann-Pick C2 protein, and lysosomal cholesterol accumulation. *J. Lipid Res.* **46,** 2559–2569 (2005).
11. Sands, M. S. & Davidson, B. L. Gene therapy for lysosomal storage diseases. *Mol. Ther.* **13,** 839–849 (2006).
12. Storch, J. & Xu, Z. Niemann-Pick C2 (NPC2) and intracellular cholesterol trafficking. *Biochim. Biophys. Acta - Mol. Cell Biol. Lipids* **1791,** 671–678 (2009).
13. Cianciola, N. L., Carlin, C. R. & Kelley, T. J. Molecular pathways for intracellular cholesterol accumulation: Common pathogenic mechanisms in Niemann-Pick disease Type C and cystic fibrosis. *Arch. Biochem. Biophys.* **515,** 54–63 (2011).
14. Liao, G. *et al.* Cholesterol accumulation is associated with lysosomal dysfunction and autophagic stress in Npc1-/- mouse brain. *Am. J. Pathol.* **171,** 962–975 (2007).
15. Pacheco, C. D., Kunkel, R. & Lieberman, A. P. Autophagy in Niemann-Pick C disease is dependent upon Beclin-1 and responsive to lipid trafficking defects. *Hum. Mol. Genet.* **16,** 1495–1503 (2007).
16. Ishibashi, S., Yamazaki, T. & Okamoto, K. Association of autophagy with cholesterol-accumulated compartments in Niemann-Pick disease type C cells. *J. Clin. Neurosci.* **16,** 954–959 (2009).
17. Peake, K. B. & Vance, J. E. Defective cholesterol trafficking in Niemann-Pick C-deficient cells. *FEBS Lett.* **584,** 2731–2739 (2010).
18. Turley, S. D., Burns, D. K., Rosenfeld, C. R. & Dietschy, J. M. Brain does not utilize low density lipoprotein-cholesterol during fetal and neonatal development in the sheep. *J Lipid Res* **37,** 1953–1961 (1996).
19. Vance, J. E. & Hayashi, H. Formation and function of apolipoprotein E-containing lipoproteins in the nervous system. *Biochim. Biophys. Acta - Mol. Cell Biol. Lipids* **1801,** 806–818 (2010).
20. Nieweg, K., Schaller, H. & Pfrieger, F. W. Marked differences in cholesterol synthesis between neurons and glial cells from postnatal rats. *J. Neurochem.* **109,** 125–134 (2009).
21. Brown, M. D., Banker, G. A., Hussaini, I. M., Gonias, S. L. & VandenBerg, S. R. Low density lipoprotein receptor-related protein is expressed early and becomes restricted to a somatodendritic domain during neuronal differentiation in culture. *Elsevier* (1997).
22. Herz, J. The LDL Receptor Gene Family: (Un)Expected Signal Transducers in the Brain. *Neuron* **29,** 571–581 (2001).
23. Hayashi, H., Campenot, R. B., Vance, D. E. & Vance, J. E. Glial Lipoproteins Stimulate Axon Growth of Central Nervous System Neurons in Compartmented Cultures. *J. Biol. Chem.* **279,** 14009–14015 (2004).
24. Yu, T. & Lieberman, A. P. Npc1 Acting in Neurons and Glia Is Essential for the Formation and Maintenance of CNS Myelin. *PLoS Genet.* **9,** (2013).
25. Liao, G. *et al.* Allopregnanolone treatment delays cholesterol accumulation and reduces autophagic/lysosomal dysfunction and inflammation in Npc1-/- mouse brain. *Brain Res.* **1270,** 140–151 (2009).
26. Xu, S., Benoff, B., Liou, H. L., Lobel, P. & Stock, A. M. Structural basis of sterol binding by NPC2, a lysosomal protein deficient in Niemann-Pick type C2 disease. *J. Biol. Chem.* **282,** 23525–23531 (2007).
27. Wang, M. L. *et al.* Identification of surface residues on Niemann-Pick C2 essential for hydrophobic handoff of cholesterol to NPC1 in lysosomes. *Cell Metab.* **12,** 166–173 (2010).
28. Kwon, H. J. *et al.* Structure of N-Terminal Domain of NPC1 Reveals Distinct Subdomains for Binding and

Transfer of Cholesterol. *Cell* **137,** 1213–1224 (2009).
29. Schultz, M. L., Krus, K. L. & Lieberman, A. P. Lysosome and endoplasmic reticulum quality control pathways in Niemann-Pick type C disease. *Brain Res.* **1649,** 181–188 (2016).
30. Cianciola, N. L. & Carlin, C. R. Adenovirus RID-α activates an autonomous cholesterol regulatory mechanism that rescues defects linked to Niemann-Pick disease type C. *J. Cell Biol.* **187,** 537–552 (2009).
31. Du, X. *et al.* A role for oxysterol-binding protein-related protein 5 in endosomal cholesterol trafficking. *J. Cell Biol.* **192,** 121–135 (2011).
32. Krause, M. R. & Regen, S. L. The structural role of cholesterol in cell membranes: From condensed bilayers to lipid rafts. *Acc. Chem. Res.* **47,** 3512–3521 (2014).
33. Brown, M. S. & Goldstein, J. L. The SREBP pathway: Regulation of cholesterol metabolism by proteolysis of a membrane-bound transcription factor. *Cell* **89,** 331–340 (1997).
34. Santos-Lozano, A. *et al.* Niemann-Pick disease treatment: a systematic review of clinical trials. *Ann. Transl. Med.* **3,** 360 (2015).
35. Wraith, J. E. *et al.* Miglustat in adult and juvenile patients with Niemann-Pick disease type C: Long-term data from a clinical trial. *Mol. Genet. Metab.* **99,** 351–357 (2010).
36. Piroth, T. *et al.* Adult-onset Niemann-Pick disease type C: Rapid treatment initiation advised but early diagnosis remains difficult. *Front. Neurol.* **8,** 8–11 (2017).
37. Vanier, M. T. Niemann-Pick disease type C. *Orphanet J. Rare Dis.* **5,** 1–18 (2010).
38. Ko, D. C., Binkley, J., Sidow, A. & Scott, M. P. The integrity of a cholesterol-binding pocket in Niemann-Pick C2 protein is necessary to control lysosome cholesterol levels. *Proc. Natl. Acad. Sci.* **100,** 2518–2525 (2003).
39. Chikh, K., Vey, S., Simonot, C., Vanier, M. T. & Millat, G. Niemann-Pick type C disease: Importance of N-glycosylation sites for function and cellular location of the NPC2 protein. *Mol. Genet. Metab.* **83,** 220–230 (2004).
40. Abbott, N. J., Patabendige, A. A. K., Dolman, D. E. M., Yusof, S. R. & Begley, D. J. Structure and function of the blood-brain barrier. *Neurobiol. Dis.* **37,** 13–25 (2009).
41. Rubin, L. L. *et al.* A cell culture model of the blood-brain barrier. *J. Cell Biol.* **115,** 1725–1735 (1991).
42. Correale, J. & Villa, A. Cellular elements of the blood-brain barrier. *Neurochem. Res.* **34,** 2067–2077 (2009).
43. Helms, H. C. *et al.* In vitro models of the blood-brain barrier: An overview of commonly used brain endothelial cell culture models and guidelines for their use. *J. Cereb. Blood Flow Metab.* **36,** 862–890 (2015).
44. Brightman, M. W. & Reese, T. S. Junctions between intimately apposed cell membranes in the vertebrate brain. *J. Cell Biol.* **40,** 648–677 (1969).
45. Assmann, J. C., Körbelin, J. & Schwaninger, M. Genetic manipulation of brain endothelial cells in vivo. *Biochim. Biophys. Acta - Mol. Basis Dis.* **1862,** 381–394 (2016).
46. Wilhelm, I. & Krizbai, I. A. In vitro models of the blood-brain barrier for the study of drug delivery to the brain. *Mol. Pharm.* **11,** 1949–1963 (2014).
47. Wilhelm, I., Fazakas, C. & Krizbai, I. A. In vitro models of the blood-brain barrier. *Acta neurobiol Exp.* 113–128 (2011).
48. Choudhury, S. R. *et al.* Viral vectors for therapy of neurologic diseases. *Neuropharmacology* **120,** 63–80 (2017).
49. Gray, S. J., Woodard, K. T. & Samulski, R. J. Viral vectors and delivery strategies for CNS gene therapy. *Ther. Deliv.* **1,** 517–534 (2010).
50. Jayant, R. D. *et al.* Current status of non-viral gene therapy for CNS disorders. *Expert Opin. Drug Deliv.* **13,** 1433–1445 (2016).
51. Saraiva, J., Nobre, R. J. & Pereira de Almeida, L. Gene therapy for the CNS using AAVs: The impact of systemic delivery by AAV9. *J. Control. Release* **241,** 94–109 (2016).
52. Chiocca, E. A. *et al.* Transfer and expression of the lacZ gene in rat brain neurons mediated by herpes simplex virus mutants. *New Biol.* **2,** 739–46 (1990).
53. Diefenbach, R. J., Miranda, M., Douglas, M. W. S. & Cunningham, A. L. Transport and egress of herpes simplex virus in neurons. *Rev. Med. Virol.* **18,** 35–51 (2008).
54. Sena-Esteves, M., Saeki, Y., Fraefel, C. & Breakefield, X. O. HSV-1 amplicon vectors - Simplicity and versatility. *Mol. Ther.* **2,** 9–15 (2000).
55. Blömer, U. *et al.* Highly Efficient and Sustained Gene Transfer in Adult Neurons with a Lentivirus Vector. *Am. Soc. Microbiol.* **71,** 6641–6649 (1997).
56. Brooks, A. I. *et al.* Functional Correction of Established Central Nervous System Deficits in an Animal Model of Lysosomal Storage Disease with Feline Immunodeficiency Virus-Based Vectors. *Natl. Acad. Sci.* **99,** 6216–6221 (2002).
57. Cetin, A., Komai, S., Eliava, M. & Seeburg, P. H. Stereotaxic gene delivery in the rodent brain. *Nat. Protoc.* **1,** 3166–3173 (2007).

58. S. Hacein-Bey-Abina, C. Von Kalle, M. Schmidt, M. P. McCormack, N. Wulffraat, P. Leboulch, A. Lim, C. S. Osborne, R. Pawliuk, E. Morillon, R. Sorensen, A. Forster, P. Fraser, J. I. Cohen, G. de Saint Basile, I. Alexander, U. Wintergerst, T. Frebourg, A. A, T. H. R. LMO2-Associated Clonal T Cell Proliferation in Two Patients after Gene Therapy for SCID- X1. *Am. Assoc. Adv. Sci.* **302,** 415–419 (2003).
59. Cattoglio, C. *et al.* Hot spots of retroviral integration in human CD34+ hematopoietic cells. *Am. Soc. Hematol.* **110,** 1770–1779 (2007).
60. Barcia, C. *et al.* One-year Expression From High-capacity Adenoviral Vectors in the Brains of Animals With Pre-existing Anti-adenoviral Immunity : Clinical Implications. *Mol. Ther.* **15,** 2154–2163 (2007).
61. Smith, A. C., Poulin, K. L. & Parks, R. J. DNA Genome Size Affects the Stability of the Adenovirus Virion. *J. Virol.* **83,** 2025–2028 (2008).
62. Akli, S. *et al.* Transfer of a foreign gene into the brain using adenovirus vectors. *Nat. Genet.* **3,** 224–228 (1993).
63. Davidson, B. L., Allen, E. D., Kozarsky, K. F., Wilson, J. M. & Roessler, B. J. A model system for in vivo gene transfer into the central nervous system using an adenoviral vector. *Nat. Genet.* **3,** 219–223 (1993).
64. Wilson, J. M. Lessons learned from the gene therapy trial for ornithine transcarbamylase deficiency. *Mol. Genet. Metab.* **96,** 151–157 (2009).
65. Herrmann, A. & Grimm, D. High-Throughput Dissection of AAV-Host Interactions : The Fast and the Curious. *J. Mol. Biol.* **430,** 2626–2640 (2018).
66. Atchinson, RW; Casto, Bruce C; Hammon, W. M. Adenovirus-Associated Defective Virus Particles. *Science (80-.).* **149,** 754–756 (1965).
67. Hudry, E. & Vandenberghe, L. H. Therapeutic AAV Gene Transfer to the Nervous System: A Clinical Reality. *Neuron* **101,** 839–862 (2019).
68. Paola Leone, David Shera, Scott W.J. McPhee, Jeremy S. Francis, Edwin H. Kolodny, Larissa T. Bilaniuk, Dah-Jyuu Wang, Mitra Assadi, Olga Goldfarb6, H. Warren Goldman, Andrew Freese, Deborah Young, Matthew J. During, R. Jude Samulski, and C. G. J. Long-Term Follow-Up After Gene Therapy for Canavan Disease Paola. *Sci Transl Med* (2012).
69. Vandamme, C., Adjali, O. & Mingozzi, F. Unraveling the Complex Story of Immune Responses to AAV Vectors Trial After Trial. *Hum. Gene Ther.* **28,** 1061–1074 (2017).
70. Donsante, A. *et al.* AAV Vector Integration Sites in Mouse Hepatocellular Carcinoma. *Science (80-.).* **317,** 5–6 (2016).
71. Walia, J. S. *et al.* Long-term correction of Sandhoff disease following intravenous delivery of rAAV9 to mouse neonates. *Mol. Ther.* **23,** 414–422 (2015).
72. Zhong, L. *et al.* Recombinant Adeno-Associated Virus Integration Sites in Murine Liver After Ornithine Transcarbamylase Gene Correction. *Hum. Gene Ther.* **24,** 520–525 (2013).
73. Deyle, D. R., Russell, D. W. & Russell, D. W. Adeno-associated virus vector integration. *Curr. Opin. Mol. Ther.* **11,** 442–447 (2009).
74. Duan, D. *et al.* Circular intermediates of recombinant adeno-associated virus have defined structural characteristics responsible for long-term episomal persistence in muscle tissue. *J Virol* **72,** 8568–8577 (1998).
75. Gao, G. *et al.* Clades of Adeno-Associated Viruses Are Widely Disseminated in Human Tissues. *J. Virol.* **78,** 6381–6388 (2004).
76. *ClinicalTrials.gov Identifier: NCT02240407 (re-administration of rAAV9-DES-hGAA injected intramuscularly)*.
77. *ClinicalTrials.gov Identifier: NCT03306277 (AVXS-101 (AAV9-based) by intravenous infusion)*.
78. Chandler, R. J. *et al.* Systemic AAV9 gene therapy improves the lifespan of mice with Niemann-Pick disease, type C1. *Hum. Mol. Genet.* **26,** 52–64 (2017).
79. Xie, C., Gong, X.-M., Luo, J., Li, B.-L. & Song, B.-L. AAV9-NPC1 significantly ameliorates Purkinje cell death and behavioral abnormalities in mouse NPC disease. *J. Lipid Res.* **58,** 512–518 (2017).
80. Merkel, S. F. *et al.* Trafficking of adeno-associated virus vectors across a model of the blood–brain barrier; a comparative study of transcytosis and transduction using primary human brain endothelial cells. *J. Neurochem.* **140,** 216–230 (2017).
81. Nonnenmacher, M. & Weber, T. Intracellular transport of recombinant adeno-associated virus vectors. *Nature* **19,** 649–658 (2012).
82. Xie, Q. *et al.* The atomic structure of adeno-associated virus (AAV-2), a vector for human gene therapy. *Proc. Natl. Acad. Sci.* **99,** 10405–10410 (2002).
83. Nam, H.-J. *et al.* Structure of Adeno-Associated Virus Serotype 8, a Gene Therapy Vector. *J. Virol.* **81,** 12260–12271 (2007).
84. Walters, R. W. *et al.* Structure of Adeno-Associated Virus Serotype 5. *J. Virol.* **78,** 3361–3371 (2004).
85. Srivastava, A., Lusby, E. W. & Berns, K. I. Nucleotide sequence and organization of the adeno-associated virus 2 genome. *J. Virol.* **45,** 555–64 (1983).
86. NPC intracellular cholesterol transporter 2 (NPC2), mRNA transcript variant 1 (Homo sapiens). With the

exception of uracil being substituted for thymine, mRNA corresponds to cDNA sequence and length. at <https://www.ncbi.nlm.nih.gov/nuccore/NM_001363688>
87. Lawlor, P. A., Bland, R. J., Mouravlev, A., Young, D. & During, M. J. Efficient gene delivery and selective transduction of glial cells in the mammalian brain by AAV serotypes isolated from nonhuman primates. *Mol. Ther.* **17,** 1692–1702 (2009).
88. Furman, J. L. *et al.* Targeting Astrocytes Ameliorates Neurologic Changes in a Mouse Model of Alzheimer's Disease. *J. Neurosci.* **32,** 16129–16140 (2012).
89. von Jonquieres, G. *et al.* Glial Promoter Selectivity following AAV-Delivery to the Immature Brain. *PLoS One* **8,** (2013).
90. Damdindorj, L. *et al.* A comparative analysis of constitutive promoters located in adeno-associated viral vectors. *PLoS One* **9,** 1–10 (2014).
91. Hocquemiller, M., Giersch, L., Audrain, M., Parker, S. & Cartier, N. Adeno-Associated Virus-Based Gene Therapy for CNS Diseases. *Hum. Gene Ther.* **27,** 478–496 (2016).
92. Shen, S. *et al.* Terminal N-Linked Galactose Is the Primary Receptor for Adeno-associated Virus 9. *J. Biol. Chem.* **286,** 13532–13540 (2011).
93. Summerford, C. & Samulski, R. J. AAVR: A Multi-Serotype Receptor for AAV. *Mol. Ther.* **24,** 663–666 (2016).
94. Halder, S. *et al.* Structure of neurotropic adeno-associated virus AAVrh.8. *J. Struct. Biol.* **192,** 21–36 (2015).
95. Kleinschmidt, J. A. *et al.* The VP1 capsid protein of adeno-associated virus type 2 is carrying a phospholipase A2 domain required for virus infectivity. *J. Gen. Virol.* **83,** 973–978 (2015).
96. Stahnke, S. *et al.* Intrinsic phospholipase A2 activity of adeno-associated virus is involved in endosomal escape of incoming particles. *Virology* **409,** 77–83 (2011).
97. Grieger, J. C., Snowdy, S. & Samulski, R. J. Separate Basic Region Motifs within the Adeno-Associated Virus Capsid Proteins Are Essential for Infectivity and Assembly. *J. Virol.* **80,** 5199–5210 (2006).
98. Rahman, N. A. *et al.* Immortalized endothelial cell lines for in vitro blood-brain barrier models: A systematic review. *Brain Res.* **1642,** 532–545 (2016).
99. Thomsen, L. B., Burkhart, A. & Moos, T. A triple culture model of the blood-brain barrier using porcine brain endothelial cells, astrocytes and pericytes. *PLoS One* **10,** 1–16 (2015).
100. Calabria, A. R., Weidenfeller, C., Jones, A. R., De Vries, H. E. & Shusta, E. V. Puromycin-purified rat brain microvascular endothelial cell cultures exhibit improved barrier properties in response to glucocorticoid induction. *J. Neurochem.* **97,** 922–933 (2006).
101. Franke, H., Galla, H. J. & Beuckmann, C. T. Primary cultures of brain microvessel endothelial cells: A valid and flexible model to study drug transport through the blood-brain barrier in vitro. *Brain Res. Protoc.* **5,** 248–256 (2000).
102. Bowman, P. D., Ennis, S. R., Rarey, K. E., Lorris Betz, A. & Goldstein, G. W. Brain microvessel endothelial cells in tissue culture: A model for study of blood-brain barrier permeability. *Ann. Neurol.* **14,** 396–402 (1983).
103. Lamszus, K., Schmidt, N. O., Ergün, S. & Westphal, M. Isolation and culture of human neuromicrovascular endothelial cells for the study of angiogenesis in vitro. *J. Neurosci. Res.* **55,** 370–381 (1999).
104. Burkhart, A., Andresen, T. L., Aigner, A., Thomsen, L. B. & Moos, T. Transfection of primary brain capillary endothelial cells for protein synthesis and secretion of recombinant erythropoietin: a strategy to enable protein delivery to the brain. *Cell. Mol. Life Sci.* **74,** 2467–2485 (2017).
105. Abbott, N. J., Rönnbäck, L. & Hansson, E. Astrocyte-endothelial interactions at the blood-brain barrier. *Nat. Rev. Neurosci.* **7,** 41–53 (2006).
106. Thomsen, M. S., Birkelund, S., Burkhart, A., Stensballe, A. & Moos, T. Synthesis and deposition of basement membrane proteins by primary brain capillary endothelial cells in a murine model of the blood–brain barrier. *J. Neurochem.* **140,** 741–754 (2017).
107. Hoheisel, D. *et al.* Hydrocortisone reinforces the blood-brain barrier properties in a serum free cell culture system. *Biochem. Biophys. Res. Commun.* **244,** 312–316 (1998).
108. Gaillard, P. J. & De Boer, A. G. Relationship between permeability status of the blood-brain barrier and in vitro permeability coefficient of a drug. *Eur. J. Pharm. Sci.* **12,** 95–102 (2000).
109. Srinivasan, B., Kolli, A. R. & Esch, M. B. TEER measurement techniques for in vitro barrier model systems. *J Lab Autom.* **20,** 107–126 (2015).
110. Greiffenberg, L. *et al.* Interaction of Listeria monocytogenes with human brain microvascular endothelial cells: InlB-dependent invasion, long-term intracellular growth, and spread from macrophages to endothelial cells. *Infect. Immun.* **66,** 5260–5267 (1998).
111. Burkhart, A. *et al.* Transfection of brain capillary endothelial cells in primary culture with defined blood–brain barrier properties. *Fluids Barriers CNS* **12,** 19 (2015).
112. Robert, M. A. *et al.* Manufacturing of recombinant adeno-associated viruses using mammalian expression

platforms. *Biotechnol. J.* **12,** (2017).
113. pAdDeltaF6, plasmid #112867. at <https://www.addgene.org/112867/>
114. Pfaffl, M. W. A new mathematical model for relative quantification in real-time RT-PCR. *Nucleic Acids Res.* **29,** e45 (2001).
115. Fan, F. & Wood, K. V. Bioluminescent Assays for High-Throughput Screening. *Assay Drug Dev. Technol.* **5,** 127–136 (2007).
116. AAV Purification by Iodixanol Gradient Ultracentrifugation. at <https://www.addgene.org/protocols/aav-purification-iodixanol-gradient-ultracentrifugation/>
117. Lock, M. *et al.* Rapid, Simple, and Versatile Manufacturing of Recombinant Adeno-Associated Viral Vectors at Scale. *Hum. Gene Ther.* **21,** 1259–1271 (2010).
118. Michelfelder, S. *et al.* Peptide ligands incorporated into the threefold spike capsid domain to re-direct gene transduction of AAV8 and AAV9 in vivo. *PLoS One* **6,** (2011).
119. Körbelin, J. *et al.* A brain microvasculature endothelial cell-specific viral vector with the potential to treat neurovascular and neurological diseases. *EMBO Mol. Med.* **8,** 609–625 (2016).
120. François, A. *et al.* Accurate Titration of Infectious AAV Particles Requires Measurement of Biologically Active Vector Genomes and Suitable Controls. *Mol. Ther. Methods Clin. Dev.* **10,** 223–236 (2018).
121. Lucey, B. P., Nelson-Rees, W. A. & Hutchins, G. M. Historical Perspective Henrietta Lacks, HeLa Cells, and Cell Culture Contamination. *Arch. Pathol. Lab. Med.* **133,** 1463–1467 (2009).
122. Hammond, S. L., Leek, A. N., Richman, E. H. & Tjalkens, R. B. Cellular selectivity of AAV serotypes for gene delivery in neurons and astrocytes by neonatal intracerebroventricular injection. *PLoS One* **12,** 1–23 (2017).
123. Lukashchuk, V., Lewis, K. E., Coldicott, I., Grierson, A. J. & Azzouz, M. AAV9-mediated central nervous system–targeted gene delivery via cisterna magna route in mice. *Mol. Ther. Methods Clin. Dev.* **3,** 15055 (2016).
124. Nakagawa, S. *et al.* A new blood-brain barrier model using primary rat brain endothelial cells, pericytes and astrocytes. *Neurochem. Int.* **54,** 253–263 (2009).
125. Worzfeld, T. & Schwaninger, M. Apicobasal polarity of brain endothelial cells. *J. Cereb. Blood Flow Metab.* **36,** 340–362 (2016).
126. Heglund, I. F., Michelet, A. A., Blazak, W. F., Furuhama, K. & Holtz, E. Preclinical pharmacokinetics and general toxicology of iodixanol. *Acta Radiol. Suppl.* **399,** 69–82 (1995).
127. Brooks, T. A. & Hawkinds, B. T. Chronic inflammatory pain leads to increased blood-brain barrier permeability and tight junction protein alterations. *Am J Physiol Hear. Circ Physiol.* **118,** 6072–6078 (2005).
128. Brooks, T. A. *et al.* Biphasic cytoarchitecture and functional changes in the BBB induce by chronic inflammatory pain. *Brain Res.* **1120,** 172–182 (2006).
129. Kim, J. Y., Ko, A. R., Hyun, H. W. & Kang, T. C. ETB receptor-mediated MMP-9 activation induces vasogenic edema via ZO-1 protein degradation following status epilepticus. *Neuroscience* **304,** 355–367 (2015).
130. Miner, J. J. & Diamond, M. S. Mechanisms of restriction of viral neuroinvasion at the blood-brain barrier. **118,** 6072–6078 (2016).
131. Miner, J. J. & Diamond, M. S. Mechanisms of restriction of viral neuroinvasion at the blood-brain barrier. *Curr Opin Immunol* **118,** 6072–6078 (2016).
132. Ryan C. Winger, Jennifer E. Koblinski, Takashi Kanda, Richard M. Ransohoff, and W. A. M. Rapid Remodeling of Tight Junctions During Paracellular Diapedesis in a Human Model of the Blood-Brain Barrier. *J Immunol.* **193,** 2427–2437 (2014).
133. Kotin, R. M. *et al.* Site-Specific Integration by Adeno-Associated Virus. *PNAS* **87,** 2211–2215 (1990).
134. R. J. Samulski, X. Zhu, X. Xiao, J.D. Brook, D. E. Housman, N. Epstein, L. A. H. Targeted integration of adeno-associated virus (AAV) into human chromosome 19. *EMBO J.* **10,** 3941–3950 (1991).
135. Young, S. M. *et al.* Roles of Adeno-Associated Virus Rep Protein and Human Chromosome 19 in Site-Specific Recombination. *J. Virol.* **74,** 3953–3966 (2000).
136. Niwa, H., Yamamura, K.-I. & Miyazaki, J.-I. Efficient selection for high-expression transfectants with a novel eukaryotic vector. *Gene* **108,** 193–199 (1991).
137. Yuhe Liu, Takashi Okada, Tatsuya Nomoto, Xiaomei Ke, Akihiro Kume, K. O. and S. X. Promoter effects of adeno-associated viral vector for transgene expression in the cochlea in vivo. *Exp. Mol. Med.* **39,** 170–175 (2007).
138. Powell, S. K., Rivera-Soto, R. & Gray, S. J. Viral expression cassette elements to enhance transgene target specificity and expression in gene therapy. *Discov. Med.* **19,** 49–57 (2015).
139. Miyazaki, J. *et al.* Expression vector system based on the chicken β-actin promoter directs efficient production of interleukin-5. *Gene* **79,** 269–277 (1989).
140. Yaguchi, M. *et al.* Characterization of the Properties of Seven Promoters in the Motor Cortex of Rats and Monkeys. *Hum. Gene Ther. Methods* **344,** 333–344 (2013).